

Electron-proton core drift and more

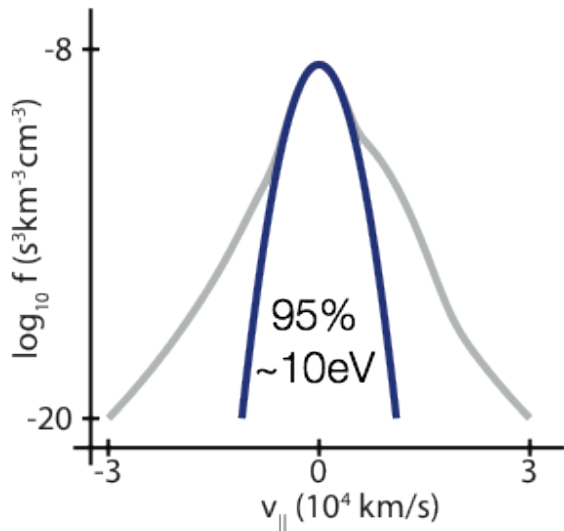
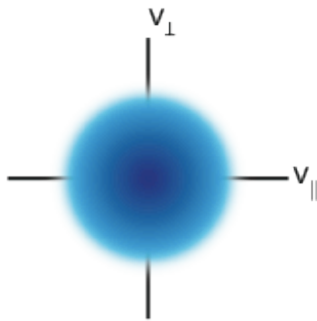
Stuart D. Bale

University of California, Berkeley

Chris Chen, Kosta Horaites, Marc Pulupa, Eliot Quataert, Chadi Salem, Yuguang Tong

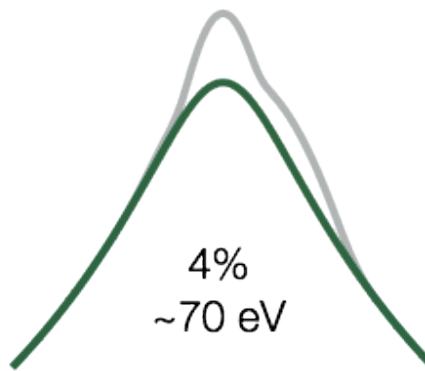
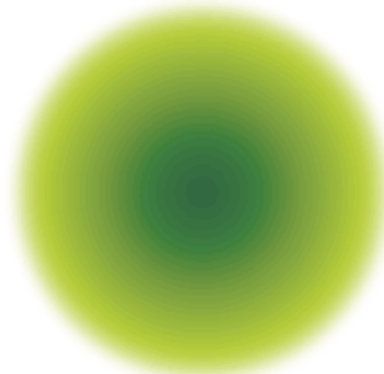
Electron distributions

Core
Maxwellian



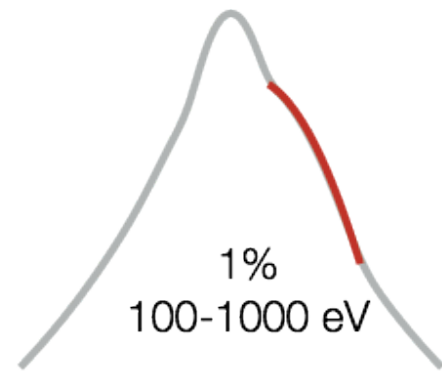
this is quasi-neutrality

Halo
Kappa



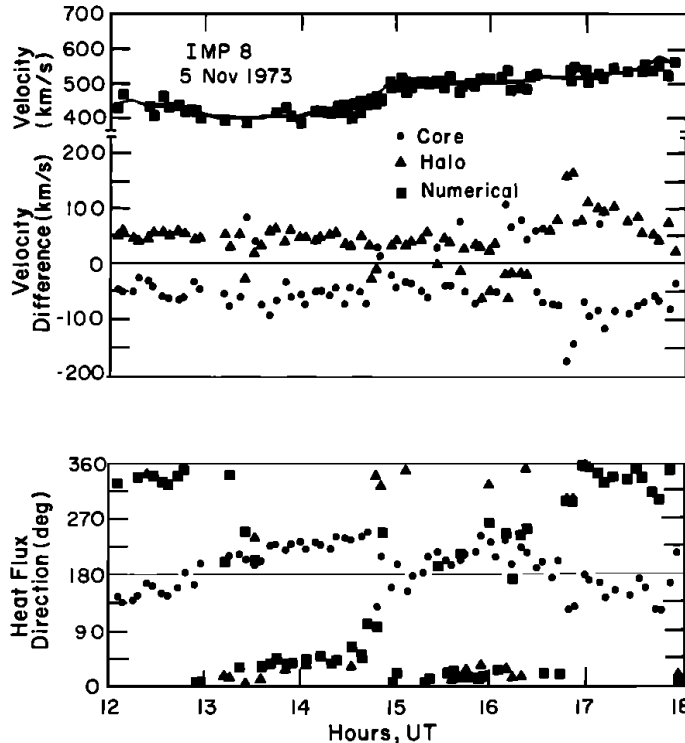
this is the corona,
p.a. scattered

Strahl
Field Aligned
Beam



this is the corona

Previous - Feldman et al., 1975



- Imp 6,7,8 spacecraft
- LANL electrostatic analyzer
- Moment calculations above ϕ_{sc}

Fig. 3. A plot of the relative core-bulk velocity and halo-bulk velocity difference vectors measured by using the Imp 8 analyzer during a velocity gradient region on November 5, 1973. Here the circles refer to the magnitude and direction of ΔV_c , and the triangles refer to the magnitude and direction of $(N_H/N_c)\Delta V_H$.

- Core drift correlates to halo drift = zero current
- V_c is $O(v_A)$

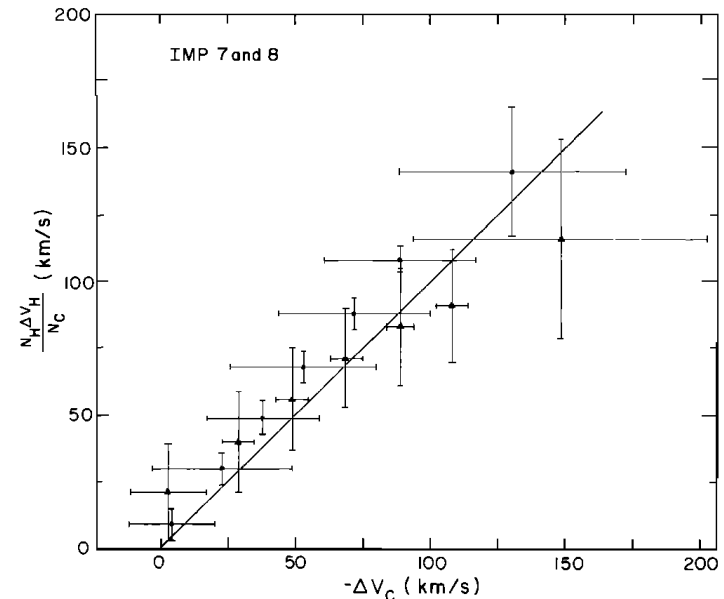


Fig. 4. The correlation between $(N_H/N_c)\Delta V_H$ and $-\Delta V_c$ using 8 months of bow shock unperturbed Imp 7 and 8 data. The format is identical to that used in Figure 2.

Previous – Gary et al., 1975

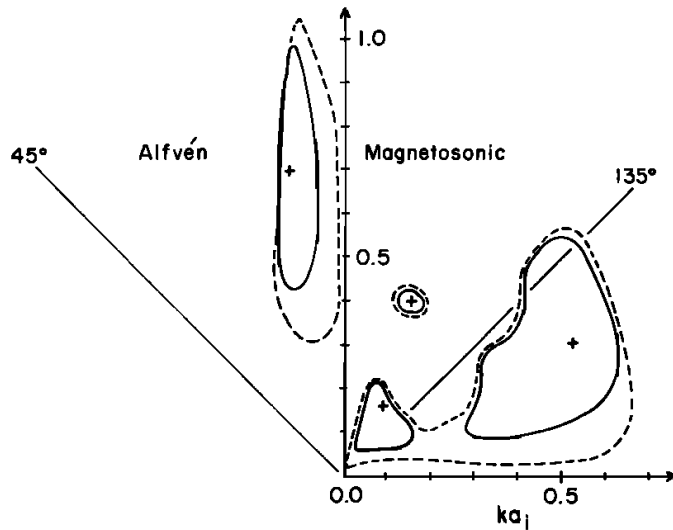


Fig. 4. Contours of constant γ as a function of wave vector \mathbf{k} . Parameters are as given in Table 1, except $v_A^2/c^2 = 2.65 \times 10^{-8}$. Here $v_{oc} = 2.42v_A$. The Alfvén instability lies at $45^\circ < \theta < 90^\circ$, the magnetosonic instability at $90^\circ < \theta < 180^\circ$, and the whistler instability is outside of the figure at $ka_i \gg 1, \theta = 180^\circ$. Dashed lines indicate $\gamma = 10^{-4}\Omega_i$; solid lines indicate $\gamma = 10^{-3}\Omega_i$; a cross denotes a local maximum in γ .

- Imp 6,7,8 spacecraft
- LANL electrostatic analyzer
- Moment calculations above ϕ_{sc}

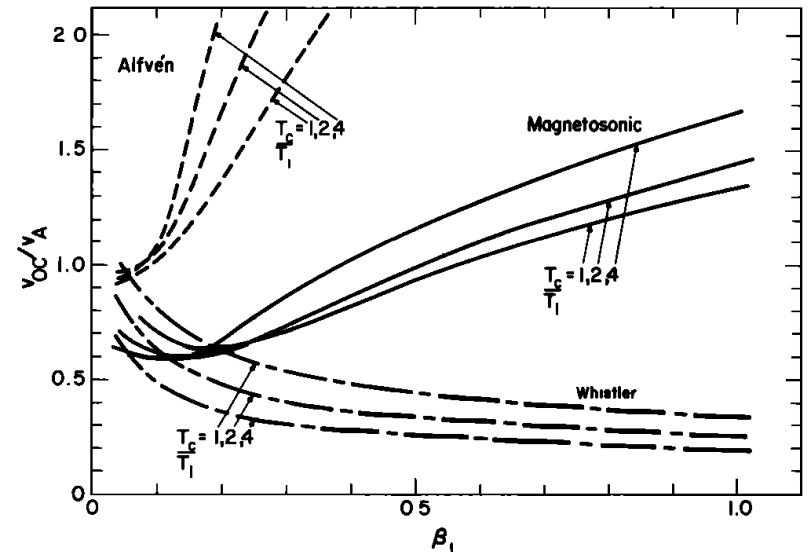


Fig. 5. Threshold core drift velocity as a function of β_i ($0.05 \leq \beta_i \leq 1.00$) with T_c/T_i variations. Parameters are as given in Table 1, except for β_i and T_c/T_i .

- Core drift correlates to halo drift = zero current

Previous – Scime et al., 1998

- Ulysses spacecraft
- LANL spher electrostatic analyzer
- 2m measurement cycle
- ϕ_{SC} is estimated from breakpoint
- Liouville correction
- Moment calculations above ϕ_{SC}
- Halo has a core-sized hole

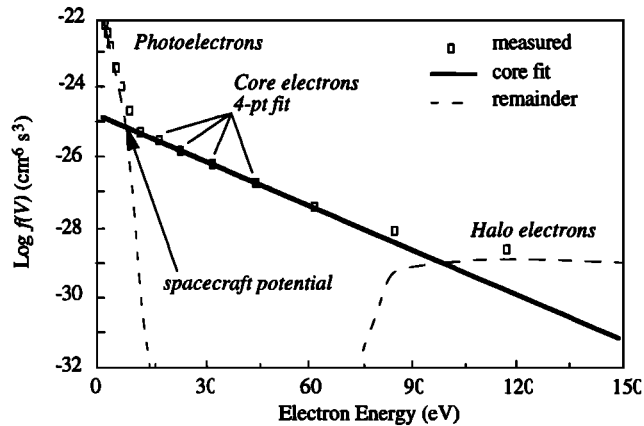


Figure 1. A typical electron distribution as measured by the electron spectrometer aboard Ulysses, after Phillips et al. [1993]. The core fit yields a temperature of 1.2×10^5 K.

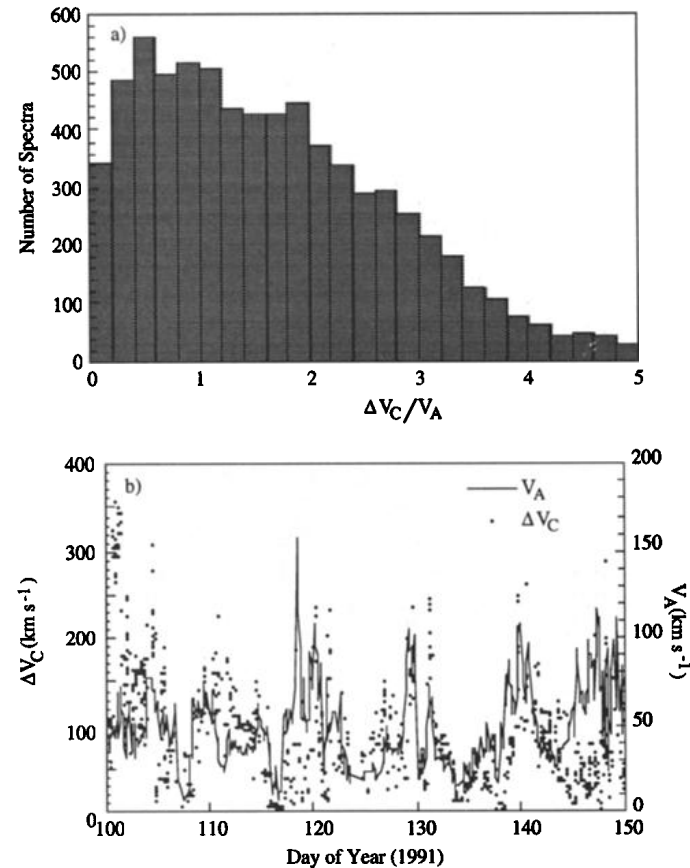


Figure 12. (a) Ratio of the core-bulk velocity difference, ΔV_C , to the local Alfvén speed. (b) Interval of Ulysses data showing intermittent correlation between the Alfvén speed and ΔV_C .

Wind/3DP measurements

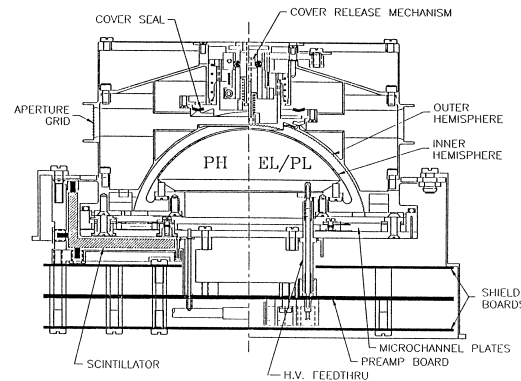
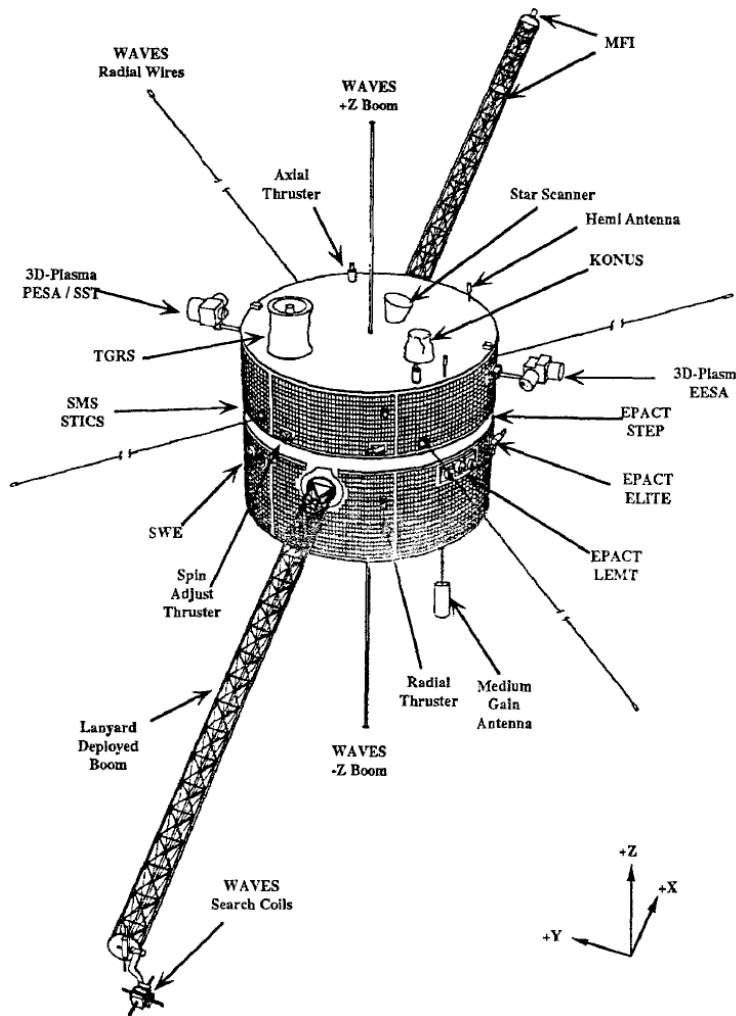


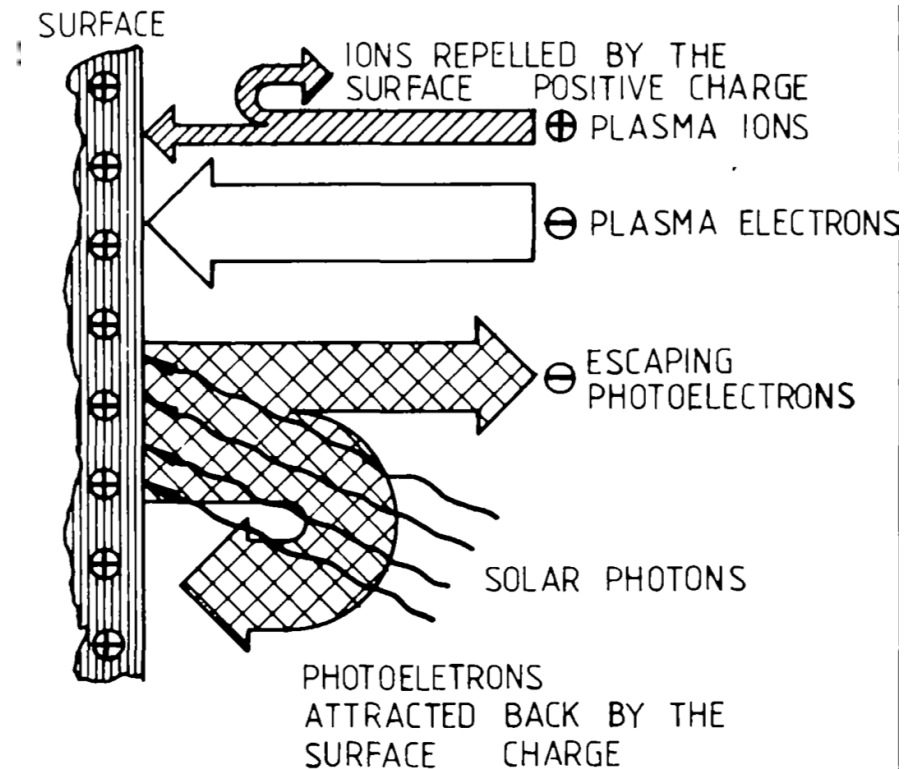
Fig. 4. Cross section of an electrostatic analyzer representative of PESA-H (left side), and PESA-L and EESA-L (right side).



- Launched in 1994, parked at L1. Lots of data
- 3 second spin period
- Superb plasma and waves measurements
- 4 ESAs (2x ion and 2x electron)
- Magnetic fields (fluxgate and search coil)
- Plasma waves and radio frequency
- Energetic particles
- Ion composition

Precision electron measurements

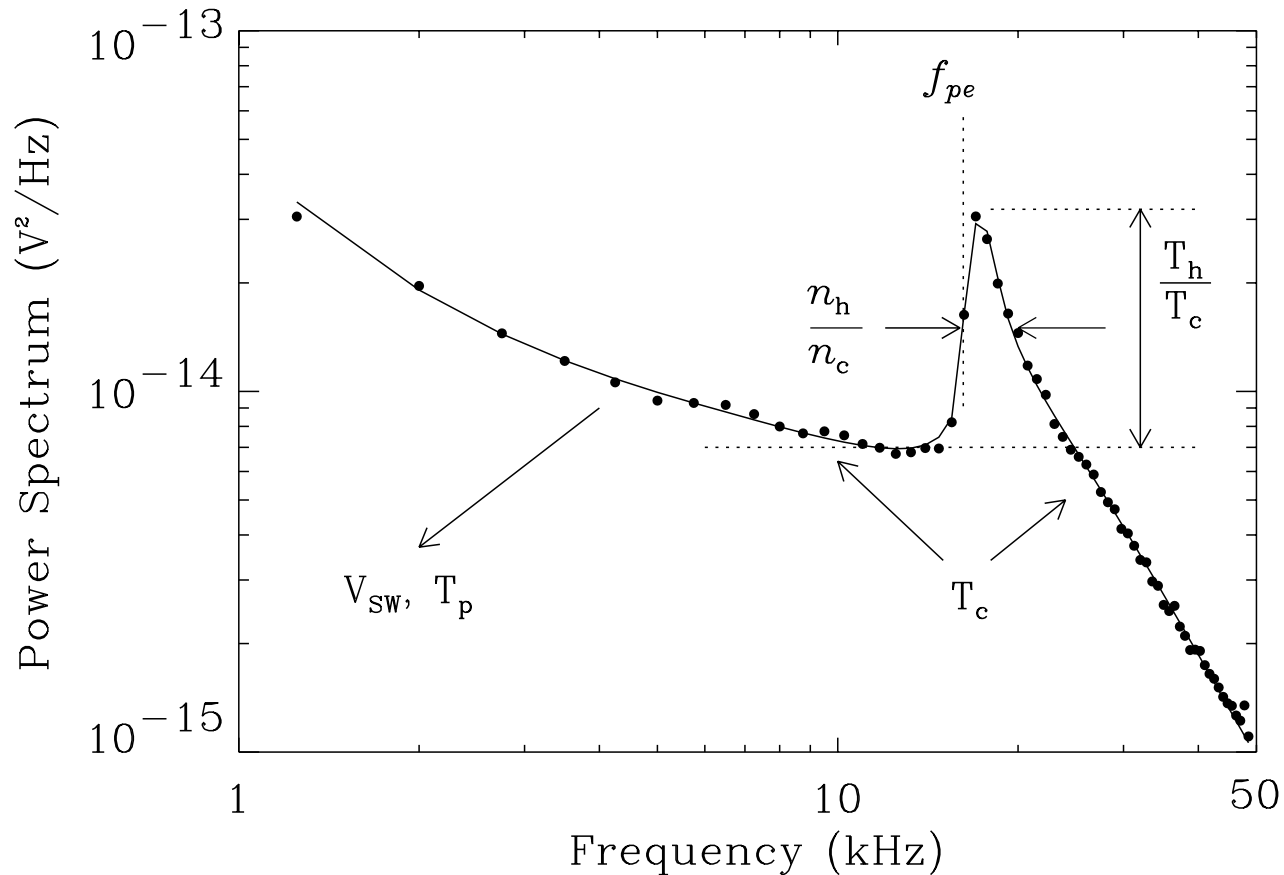
- In the solar wind, spacecraft charge slightly (a few eV) positive due to solar UV photoemission.
- Spacecraft potential affects electron parameters (N_e , T_e) measured by plasma instruments.
- Potential is dependent on N_e , T_e – which is what we want to measure!



Use quasi-thermal noise (electric fluctuation) measurements to constrain the absolute plasma density – immune to s/c plasma environment!

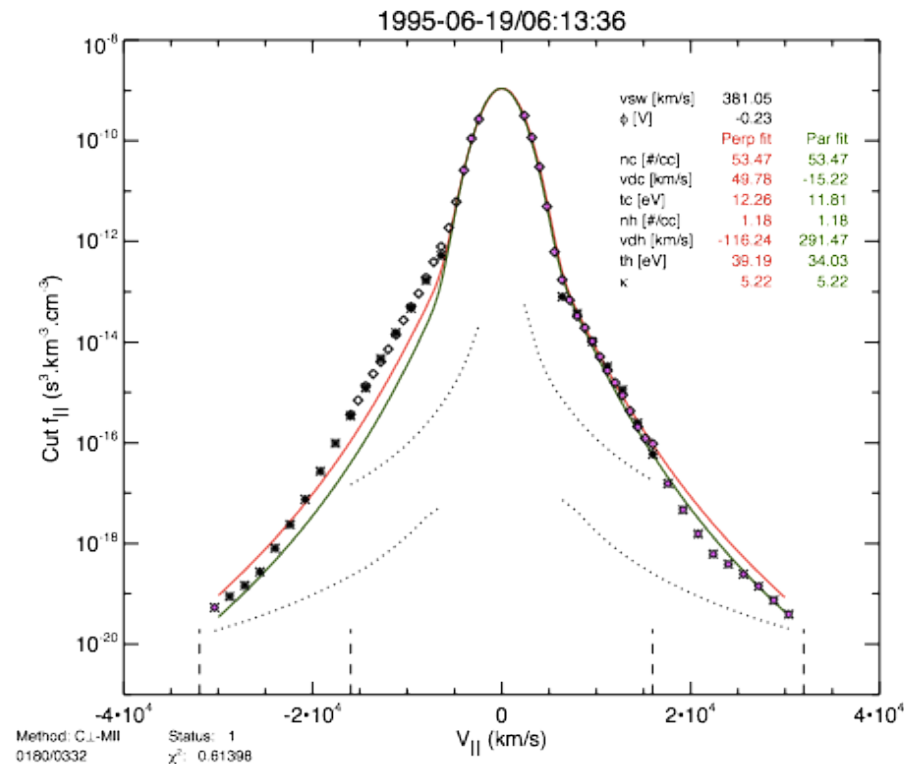
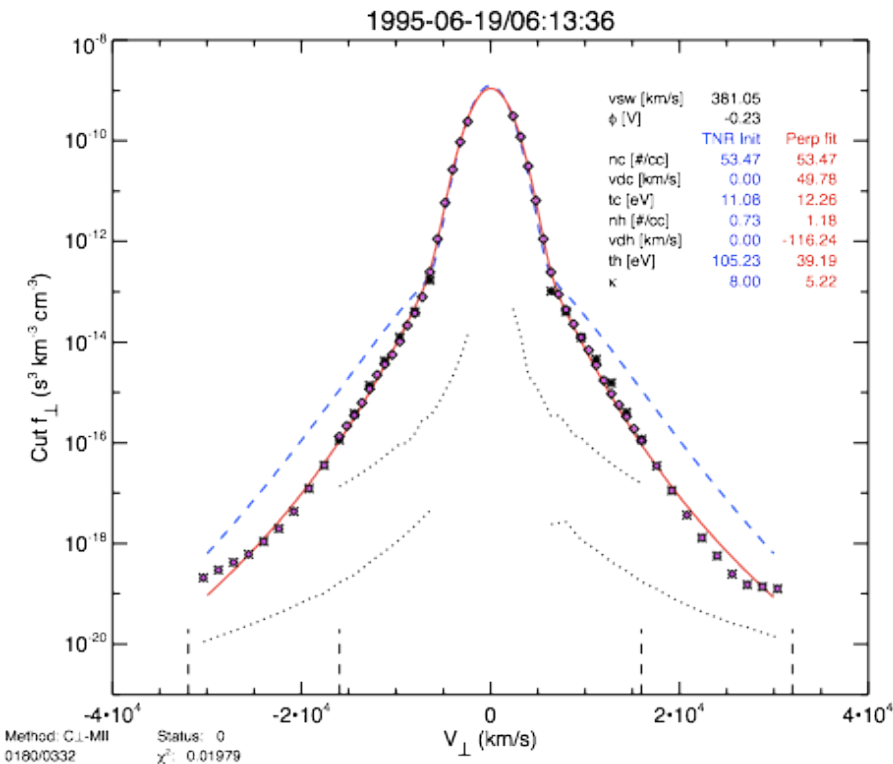
Note: 1V ~ 600 km/s for an electron

Precision electron measurements



Use **quasi-thermal noise** (electric fluctuation) measurements to constrain the absolute plasma density – immune to s/c charging effects! Requires $L \gg \lambda_D$

electron distribution function fits - 'slow wind'



- use drifting bi-Maxwellian core and drifting bi-Lorentzian halo, integrate strahl

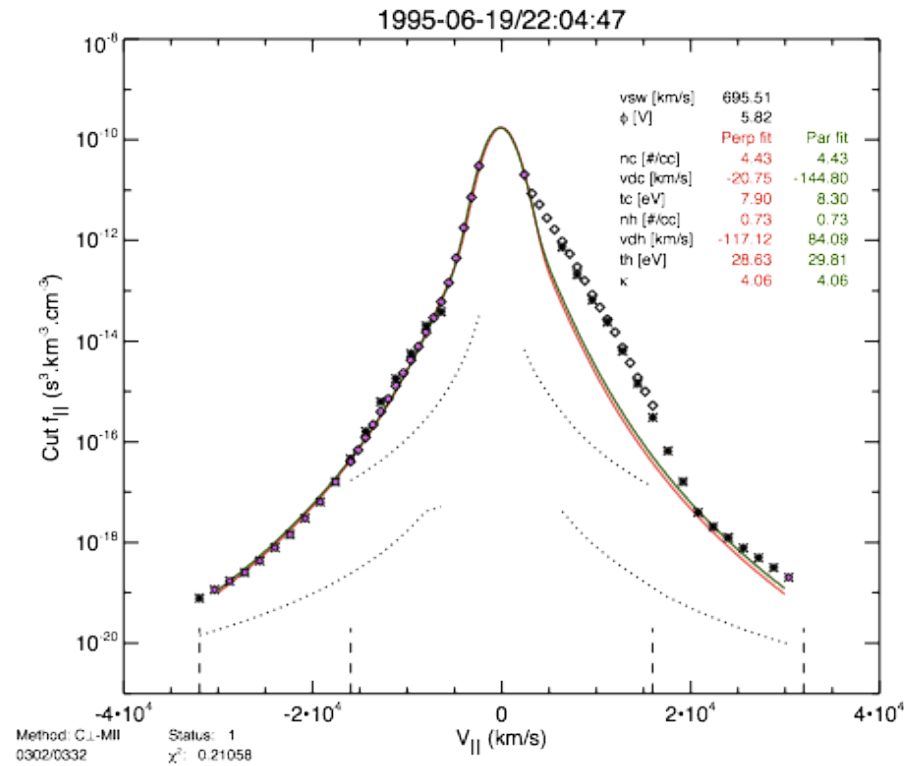
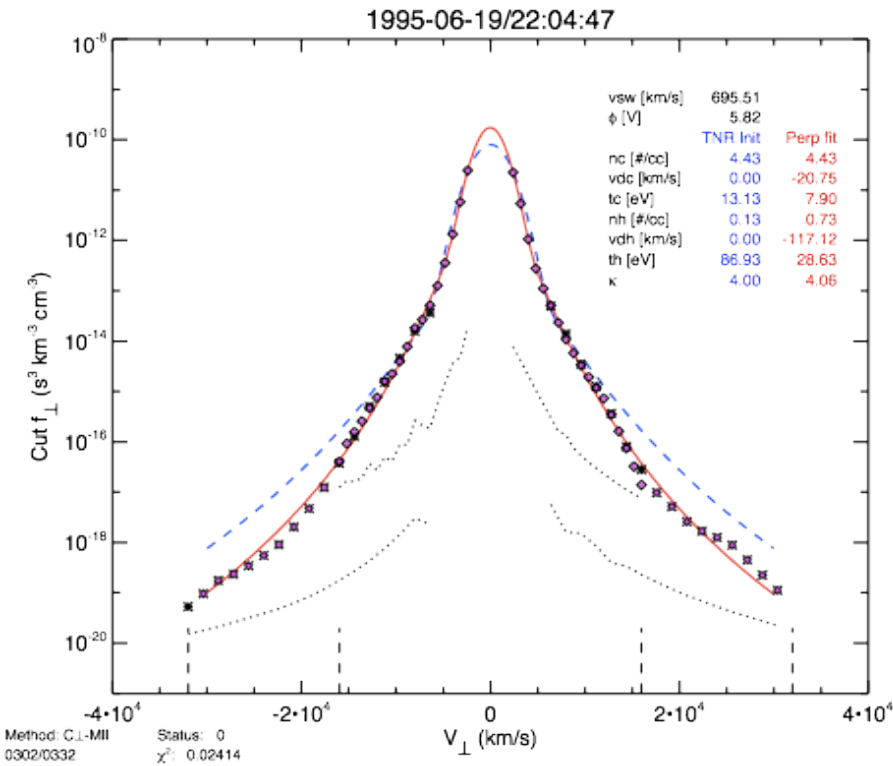
0) correct $f(v)$ for s/c potential

1) fit $f(v)$ perpendicular to core and halo - use QTN initial values

2) fit $f(v)$ parallel to core and halo - use QTN and $f(v)$ perp initial values

3) subtract $f(v)$ core and halo, fit strahl, and compute strahl moments

electron distribution function fits - 'fast wind'



- use drifting bi-Maxwellian core and drifting bi-Lorentzian halo, integrate strahl

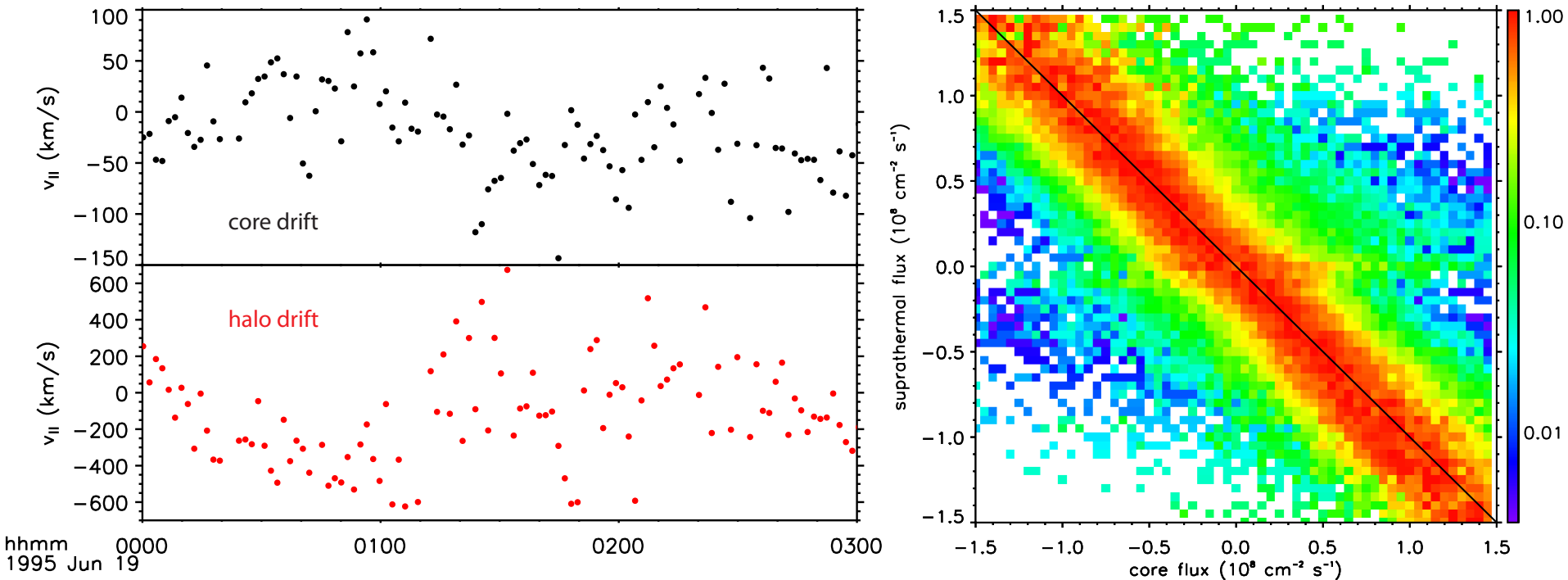
0) correct $f(v)$ for s/c potential

1) fit $f(v)$ perpendicular to core and halo - use QTN initial values

2) fit $f(v)$ parallel to core and halo - use QTN and $f(v)$ perp initial values

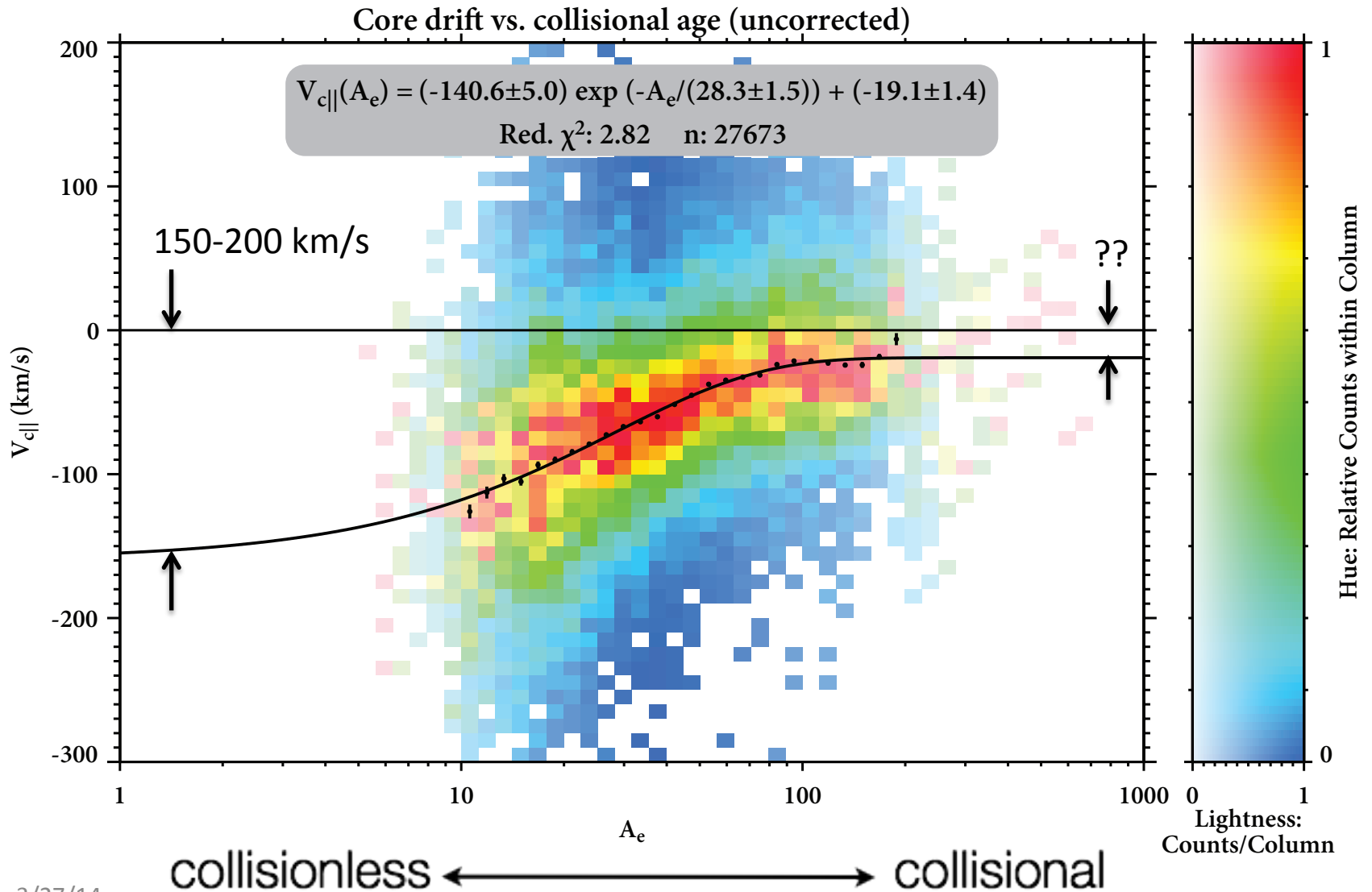
3) subtract $f(v)$ core and halo, fit strahl, and compute strahl moments

Current balance in the proton frame

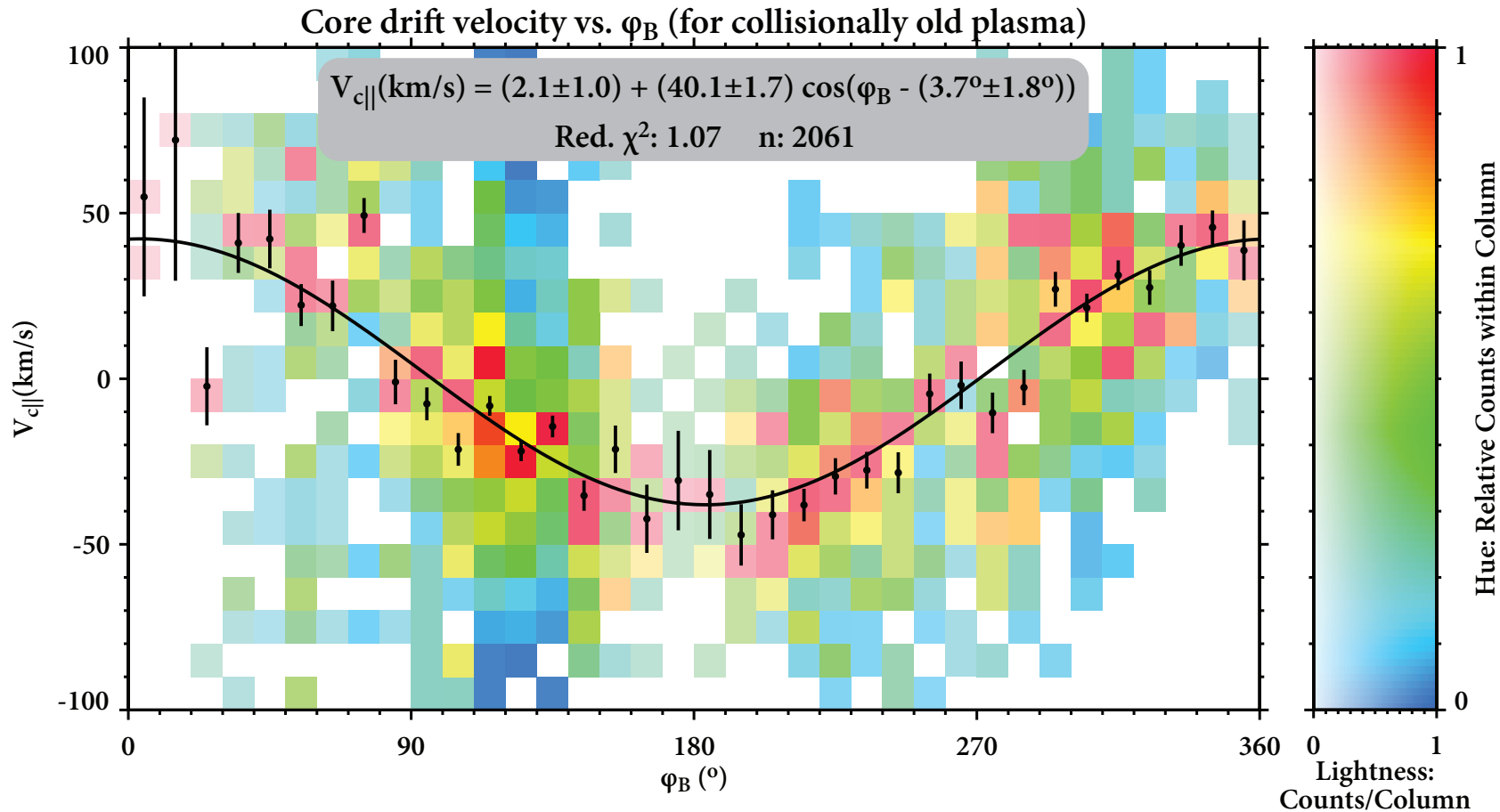


In the charge-center ($\sim \text{cm}$) frame, we expect zero net current: $n_c v_c + n_h v_h + n_s v_s = 0$, which seems to be so...

Core electron-proton (||) drift

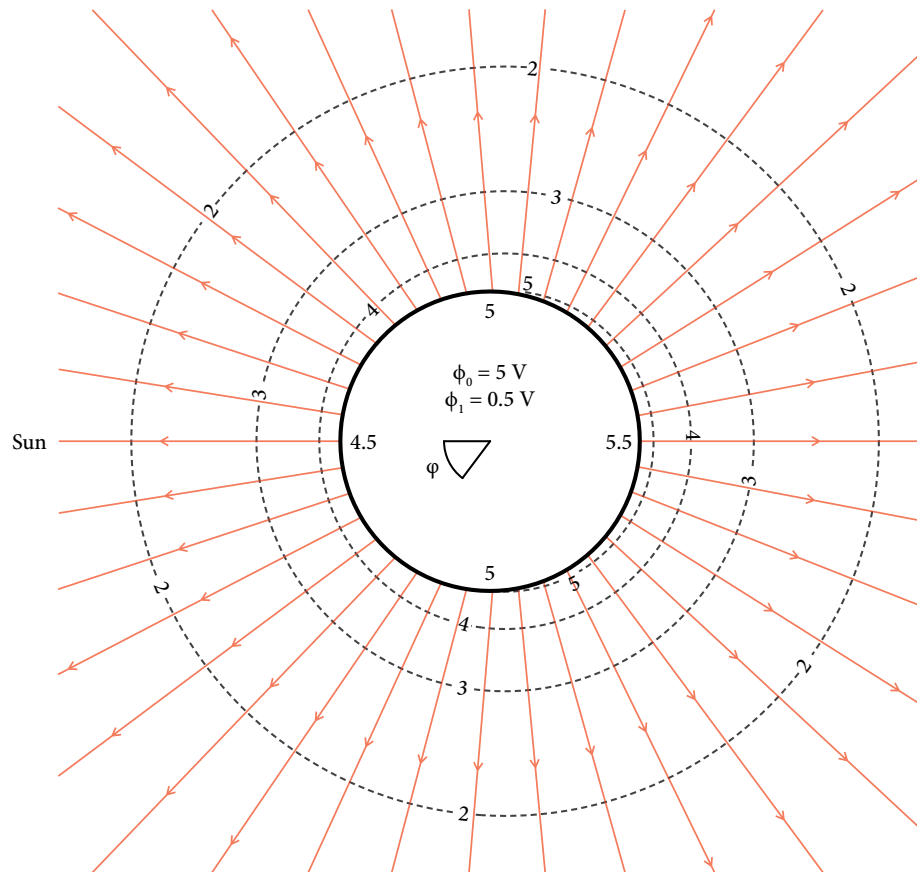


Sunward drift in collisional regime



- The remnant drift (in the field-aligned solar wind frame) varies sinusoidally with the clock angle of the magnetic field.
- Projection of a constant drift in the sunward direction, which exists independent of the IMF direction.
- We interpret this as evidence for a modulated spacecraft potential

Variation in spacecraft potential



Spatially varying structure (left) vs. spin modulation (right)

Dipole correction to s/c potential

$$\phi(\varphi, R) = K \left(\frac{1}{R} - \frac{A \cos \varphi}{R^2} \right)$$

$$\phi(\varphi) = \phi_0 - \phi_1 \cos \varphi$$

$$f'(v') = \frac{N_{e0}}{\pi^{3/2} v_{th}^3} e^{e\phi(\varphi)/k_B T_{e0}} e^{-v'^2/v_{th}^2}$$

$$N_e = 2\pi \int_0^\pi d\varphi \int_{v'_{min}(\varphi)}^\infty \sin \varphi dv' v'^2 f'(v')$$

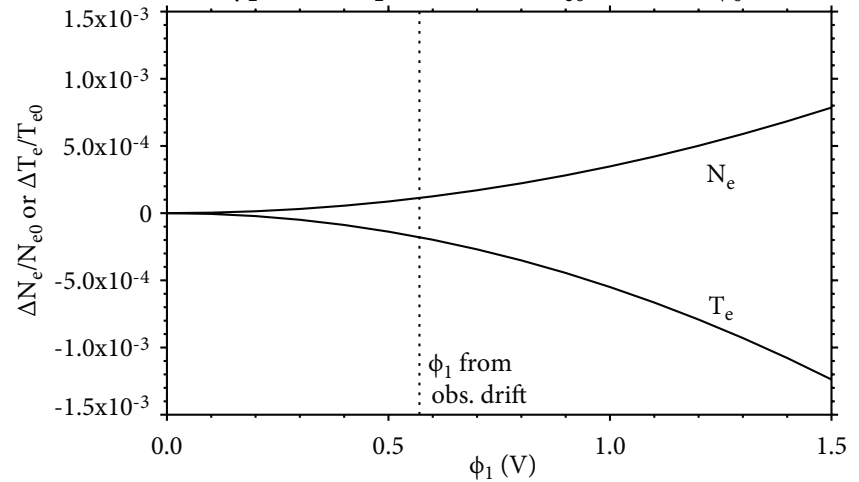
$$V_e = \frac{2\pi}{N_e} \int_0^\pi d\varphi \int_{v'_{min}(\varphi)}^\infty \sin \varphi dv' \mathbf{v}' v'^2 f'(v')$$

$$T_e = \frac{2\pi}{N_e} \frac{m_e}{3k_B} \int_0^\pi d\varphi \int_{v'_{min}(\varphi)}^\infty \sin \varphi dv' v'^4 f'(v')$$

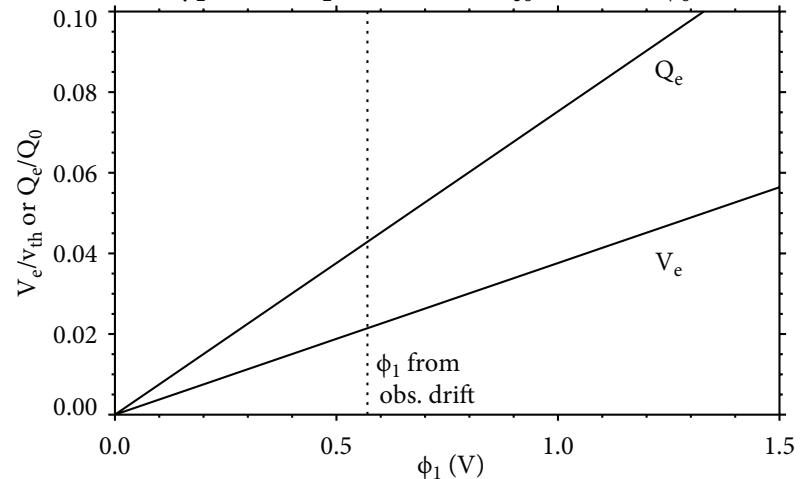
$$Q_e = 2\pi \int_0^\pi d\varphi \int_{v'_{min}(\varphi)}^\infty \sin \varphi dv' \frac{1}{2} m_e \mathbf{v}' v'^4 f'(v')$$

$$\frac{V_e}{v_{th}} = \frac{2}{3\sqrt{\pi}} \frac{e\phi_1}{k_B T_{e0}}$$

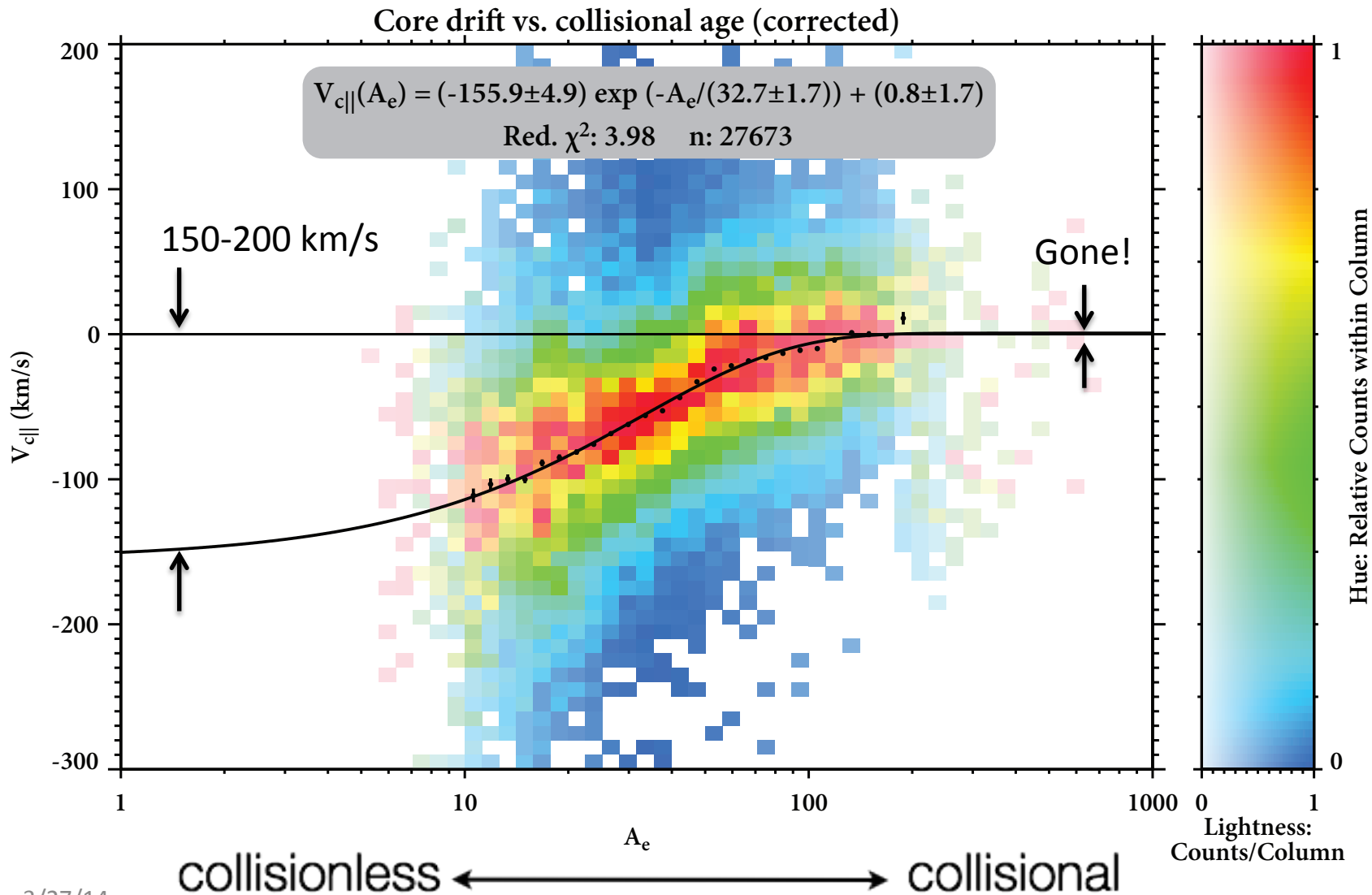
Effect of dipole term on even moments (N_e , T_e)
for typical SW parameters ($T_{e0} = 10$ eV, $\phi_0 = 5$ V)



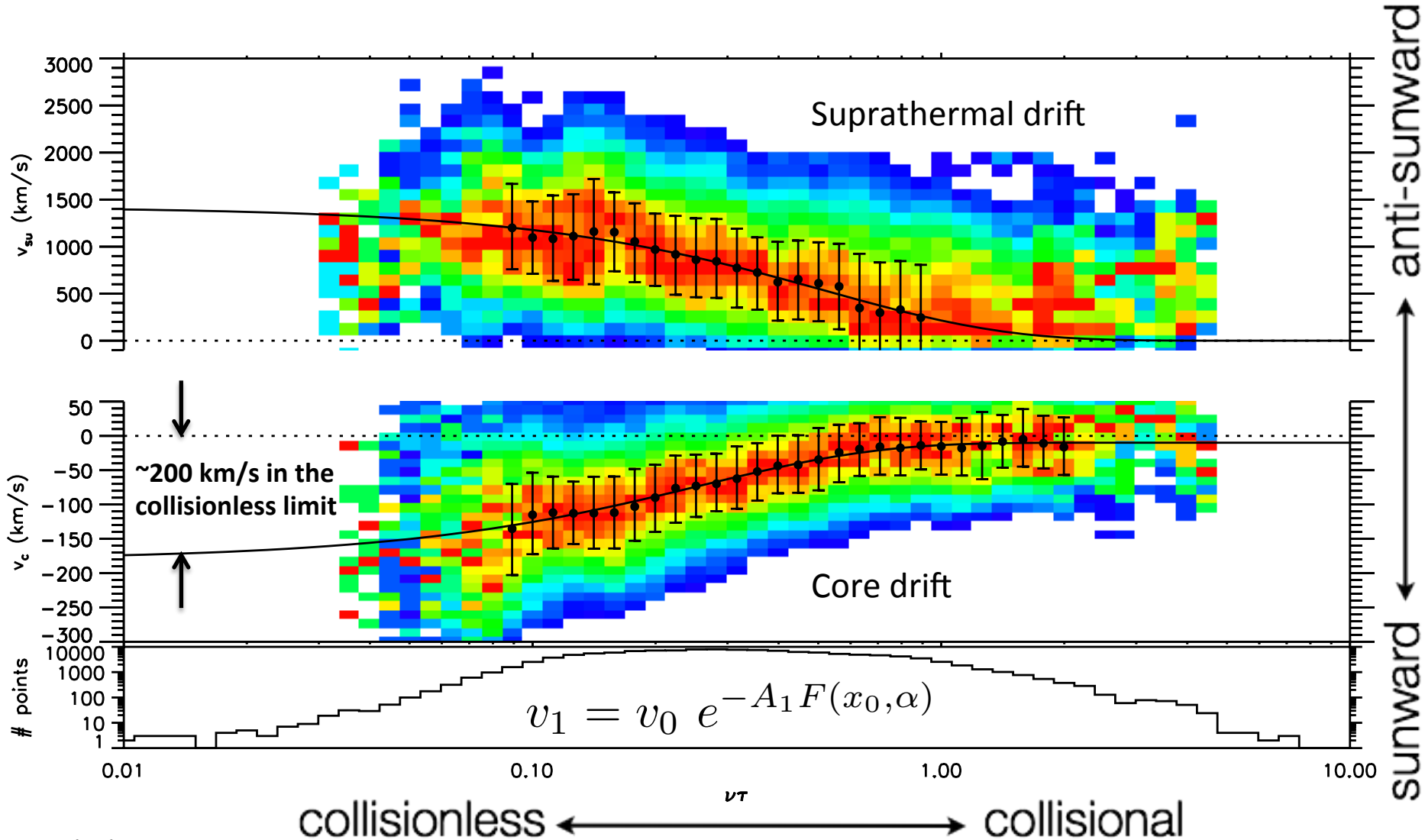
Effect of dipole term on odd moments (V_e , Q_e)
for typical SW parameters ($T_{e0} = 10$ eV, $\phi_0 = 5$ V)



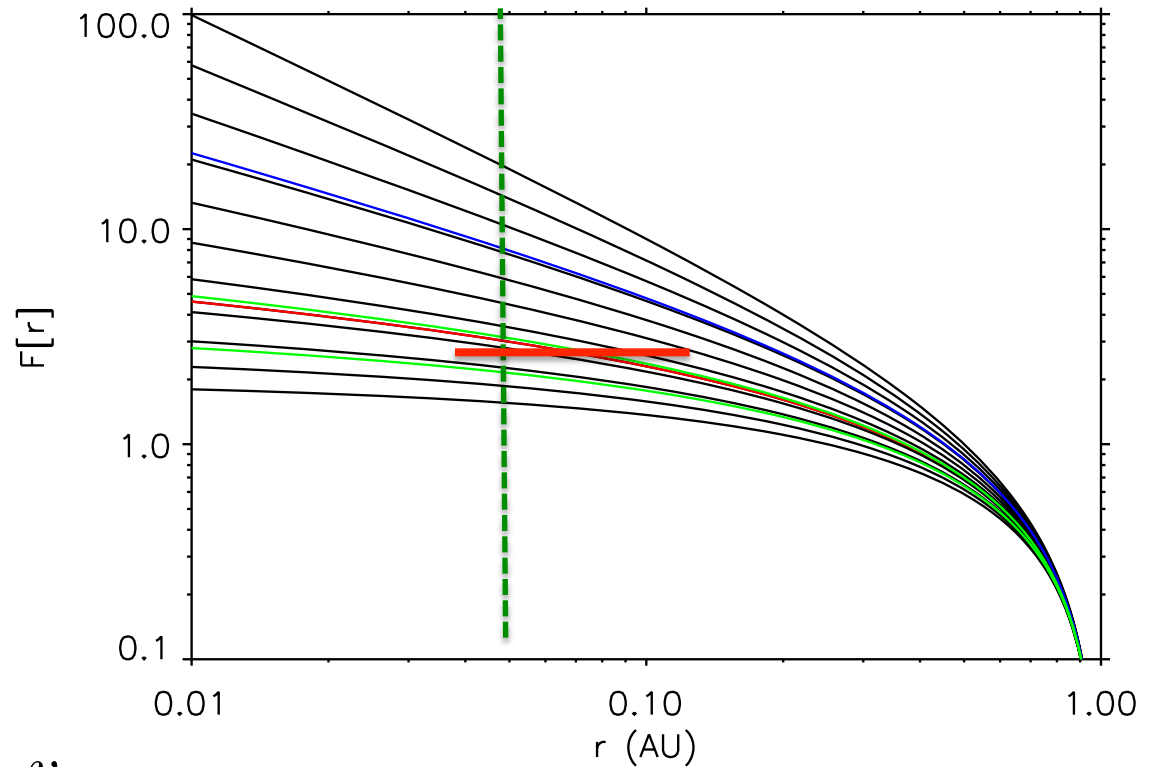
Core electron-proton (||) drift



Large electron core drifts



Larger electron core drifts in the corona



$$\frac{dv_{||}}{dt} = v \frac{\partial v_{||}}{\partial r} = -\nu(r)_s v_{||}$$

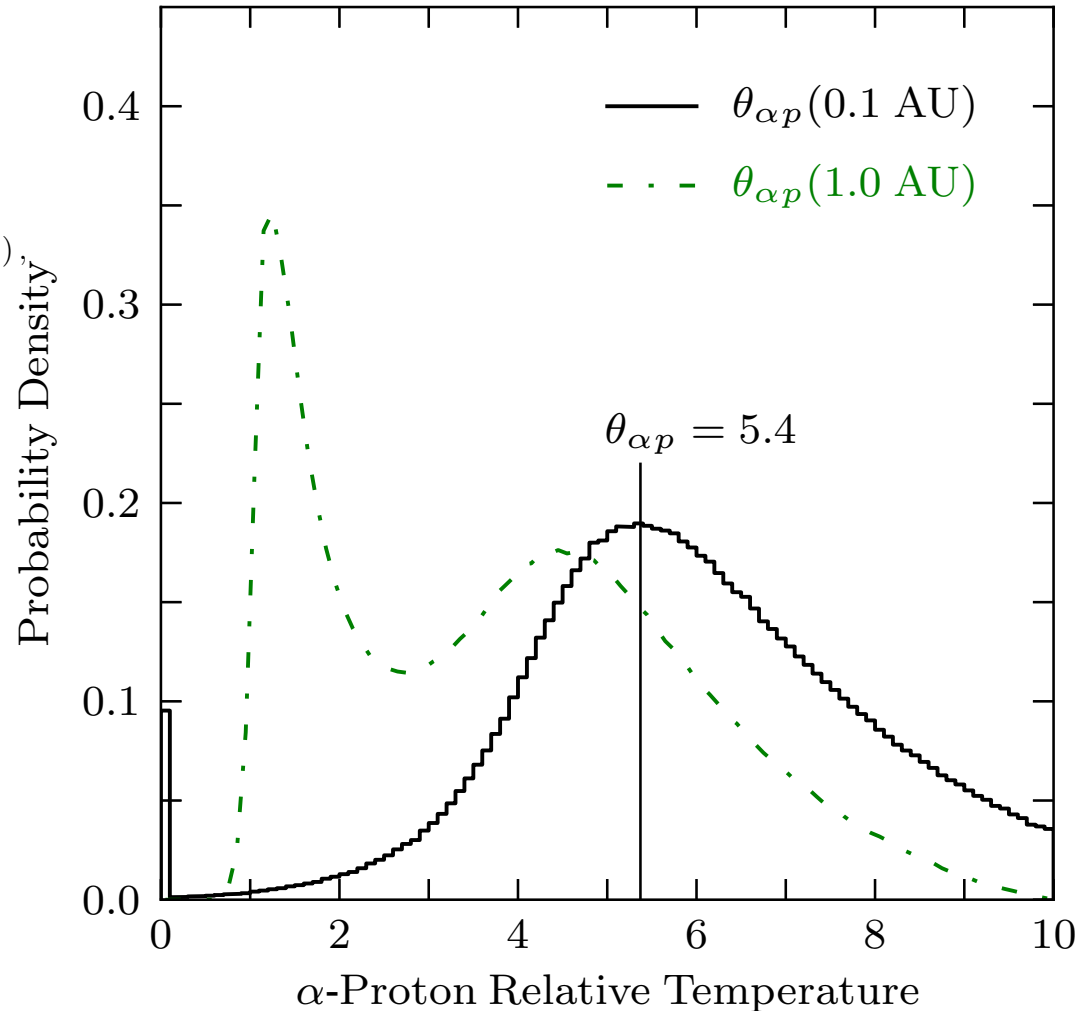
$$\log(v_1/v_0) = -\left\{ \mathcal{K} \frac{n_1}{v_{sw} T_1^{3/2}} \right\} \frac{(x_0^{\frac{3\alpha}{2}-1} - 1)}{(\frac{3\alpha}{2} - 1)} = -\mathcal{A}_1 F(x_0, \alpha)$$

Larger α/p temperature ratios in the corona

$$\frac{dT_j}{dt} = \sum_{j' \neq j} \left(0.174 \frac{\text{cm}^3 \text{K}^{3/2}}{\text{s}} \right) \left(\frac{(\mu_j \mu_{j'})^{1/2} Z_j^2 Z_{j'}^2 n_{j'} \lambda_{jj'}}{(\mu_j T_{j'} + \mu_{j'} T_j)^{3/2}} \right) (T_{j'} - T_j),$$

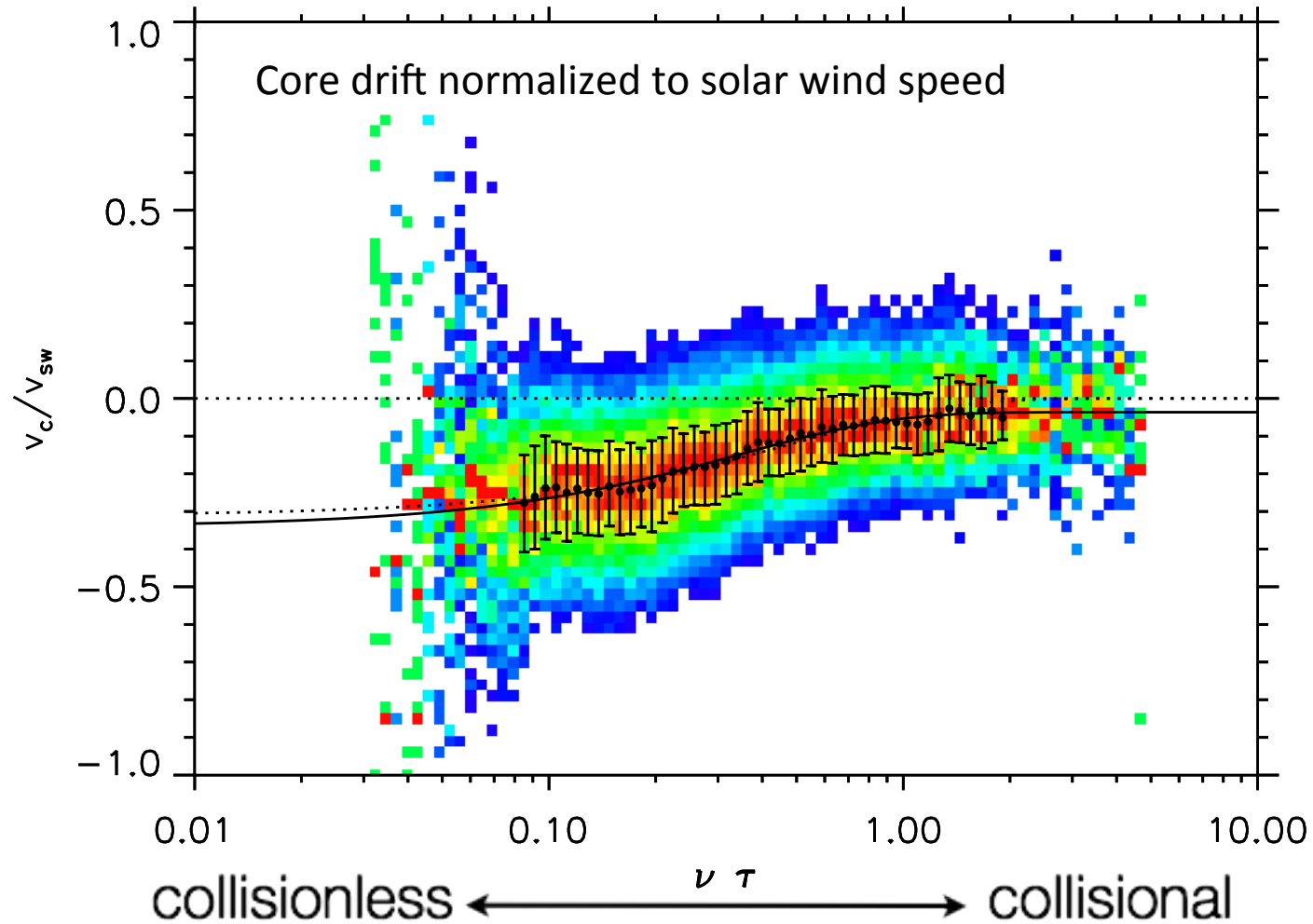
$$\frac{d\theta_{\alpha p}}{dr} = \left(2.60 \times 10^7 \frac{\text{cm}^3 \text{km K}^{3/2}}{\text{s AU}} \right) \left(\frac{n_p}{v_{rp} T_p^{3/2}} \right) \left(\frac{\mu_\alpha^{1/2} Z_\alpha^2 (1 - \theta_{\alpha p}) (1 + \eta_{\alpha p} \theta_{\alpha p})}{(\mu_\alpha + \theta_{\alpha p})^{3/2}} \right) (\lambda_{\alpha p}),$$

At 20 Rs, T_α/T_p may be entirely 'nonthermal'



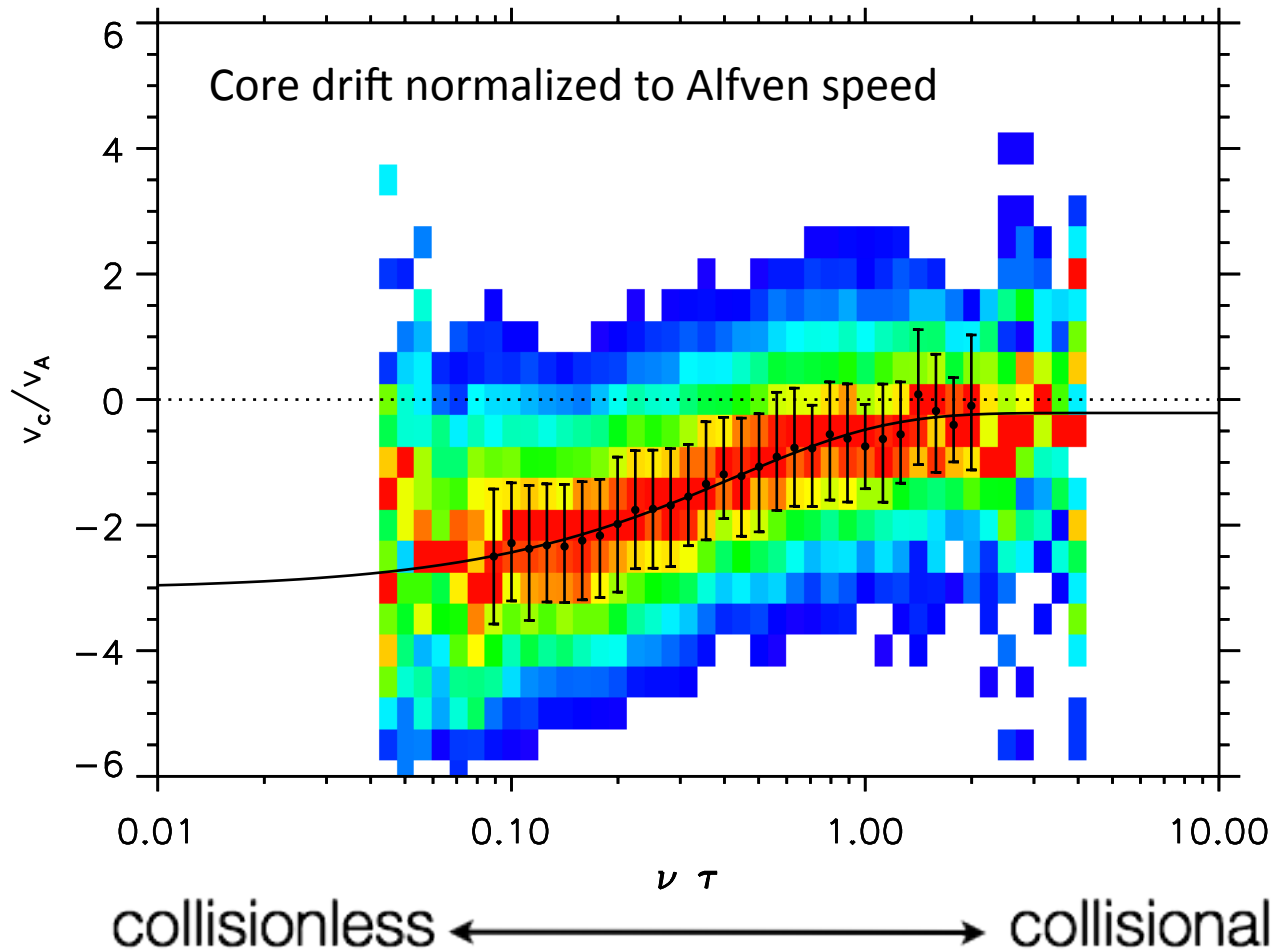
(Maruca et al., 2013)

Electron core drift to v_{sw}

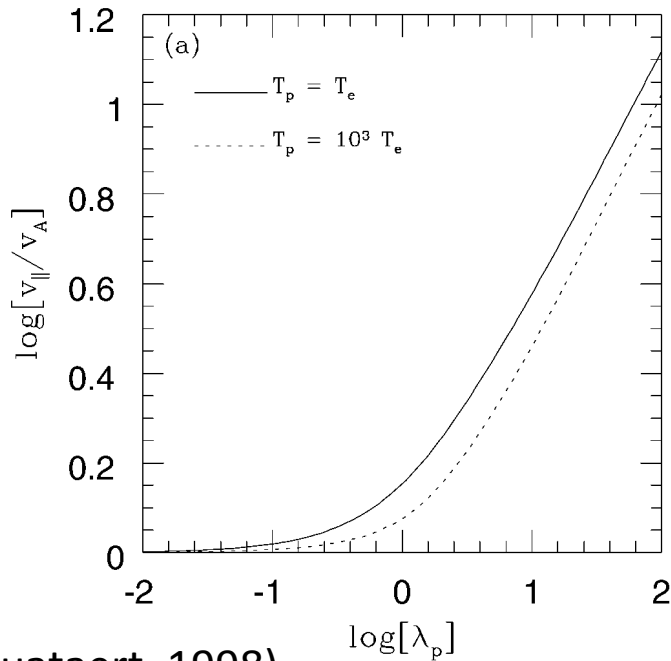


Large core drift rates exceed the Alfvén and sound speeds! This should be unstable.

Electron core drift to v_A



Large core drift rates exceed the Alfvén and sound speeds! This should be unstable.



Heating by kinetic Alfvén waves (KAW)

Linearized Vlasov-Maxwell calculation

isotropic Maxwellian protons

isotropic Maxwellian drifting core electrons

isotropic Maxwellian drifting halo electrons

current balance: $n_c v_c + n_h v_h = 0$ in proton frame

kinetic Alfvén waves – highly oblique (89°), $k \rho_i \sim 1$

‘Heating’ rate is derived from $\mathbf{E} \cdot \mathbf{j}$ (Stix, 1962)

P = energy absorbed per wave period

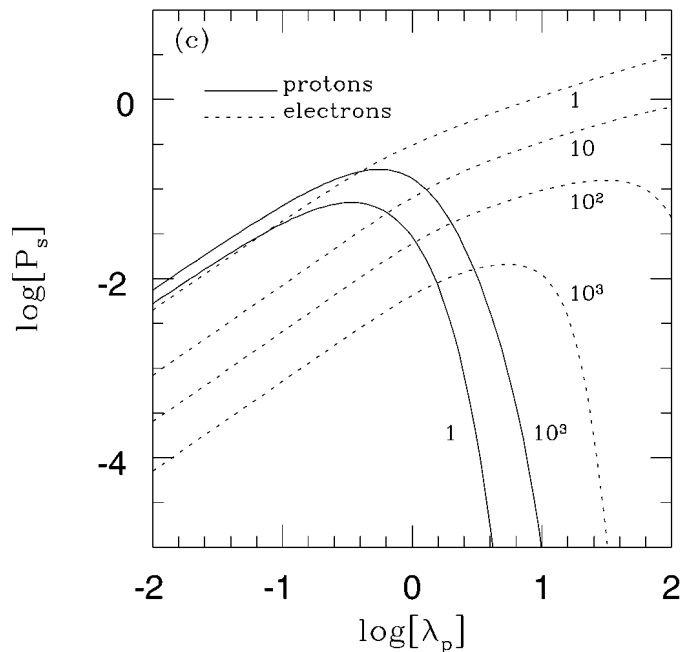
$P_s > 0$ - species s absorbs wave energy

$P_s < 0$ - species s gives energy to wave

$$P_s = \frac{\mathbf{E}^* \cdot \chi_s^a |_{\omega=\omega_r} \cdot \mathbf{E}}{4W},$$

$$W \equiv \frac{1}{16\pi} \left[\mathbf{B}^* \cdot \mathbf{B} + \mathbf{E}^* \cdot \frac{\partial}{\partial \omega} (\omega \epsilon_h) |_{\omega=\omega_r} \cdot \mathbf{E} \right]$$

(Quataert, 1998)



Instability was studied by Gary (1975)

Sunward KAW for sunward core drift

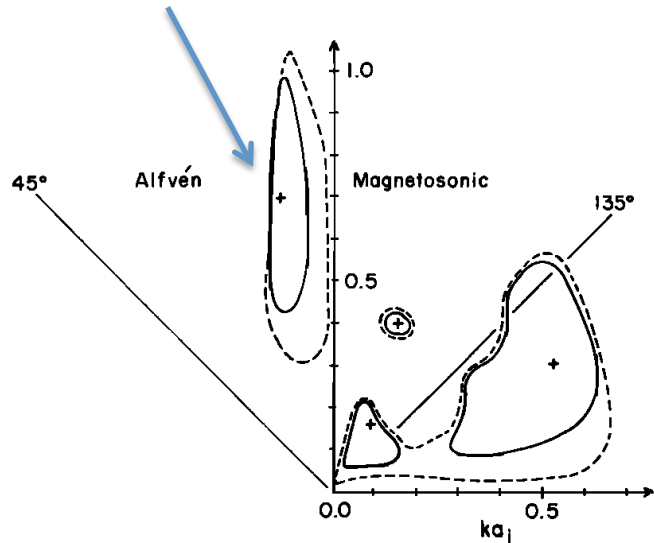
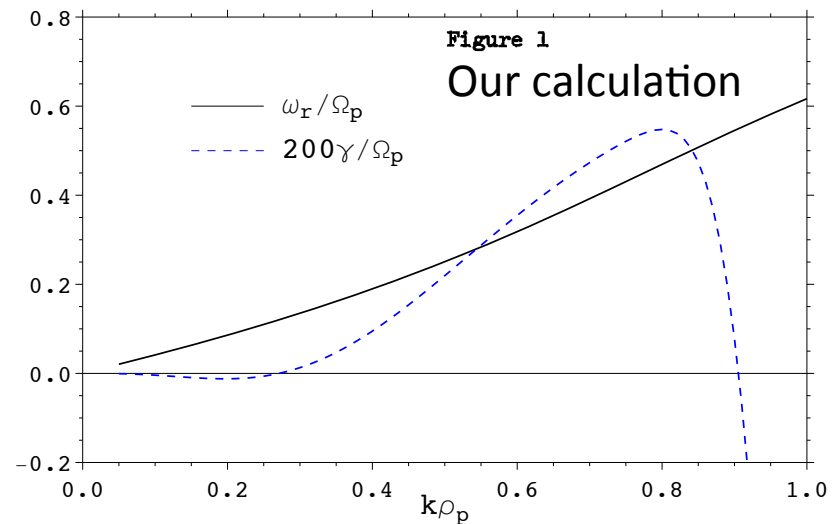
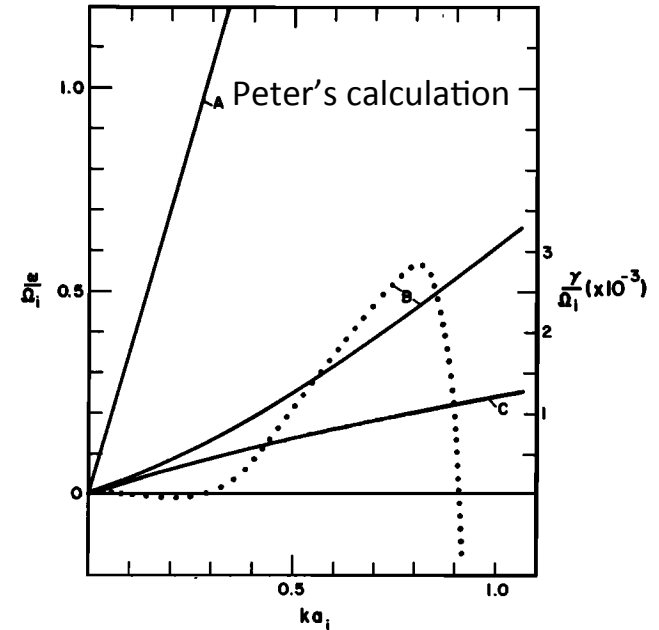


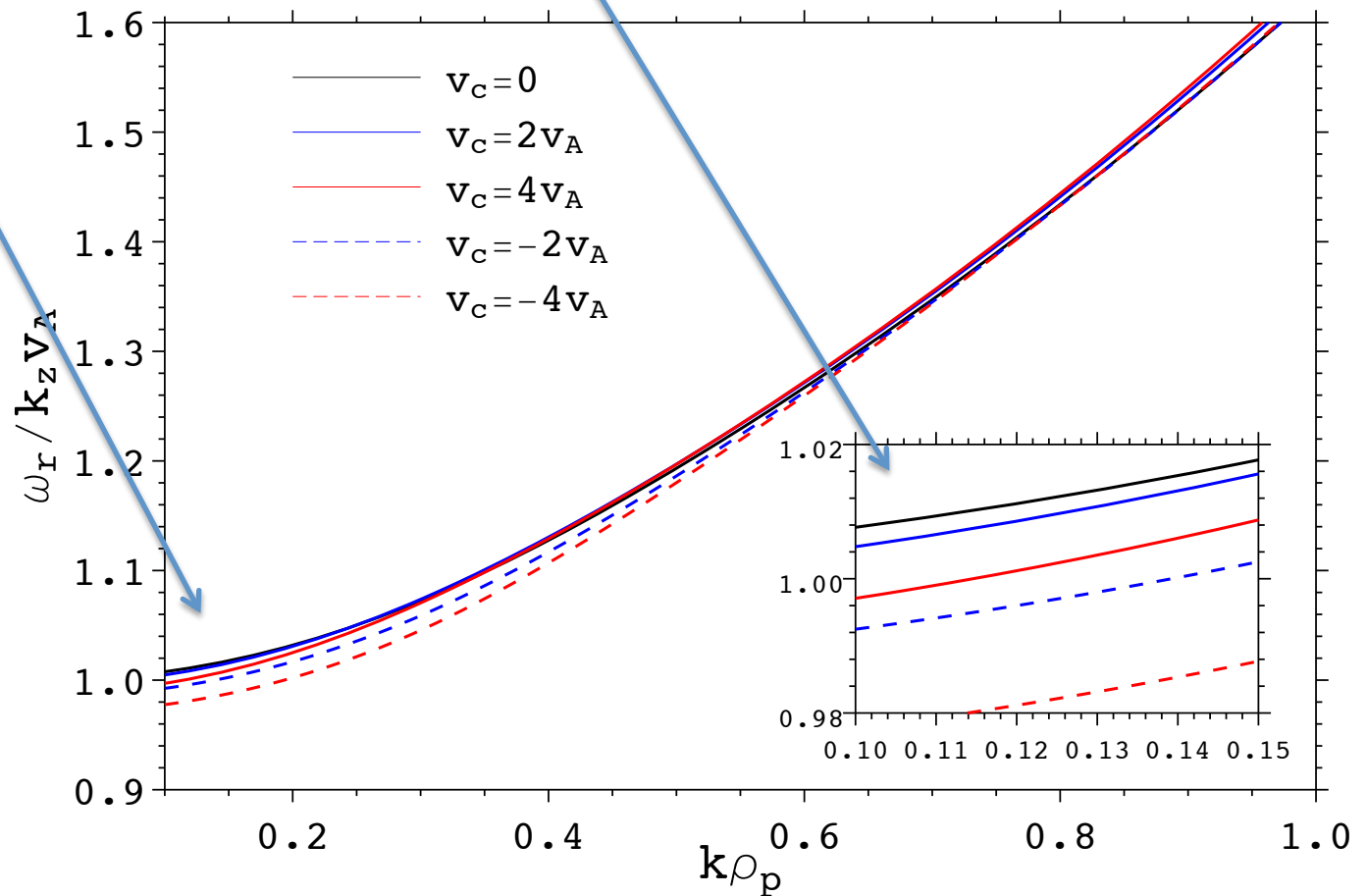
Fig. 4. Contours of constant γ as a function of wave vector \mathbf{k} . Parameters are as given in Table 1, except $v_A^2/c^2 = 2.65 \times 10^{-8}$. Here $v_{0c} = 2.42v_A$. The Alfvén instability lies at $45^\circ < \theta < 90^\circ$, the magnetosonic instability at $90^\circ < \theta < 180^\circ$, and the whistler instability is outside of the figure at $ka_i \gg 1, \theta = 180^\circ$. Dashed lines indicate $\gamma = 10^{-4}\Omega_i$; solid lines indicate $\gamma = 10^{-3}\Omega_i$; a cross denotes a local maximum in γ .

$$T_h = 12 T_c, n_c = 0.95 n_i, v_d = 2.42 v_A, \beta_i = 0.25$$



Dispersion/phase speed

Waves remain mostly in the proton frame
Few % Doppler shift at long wavelengths

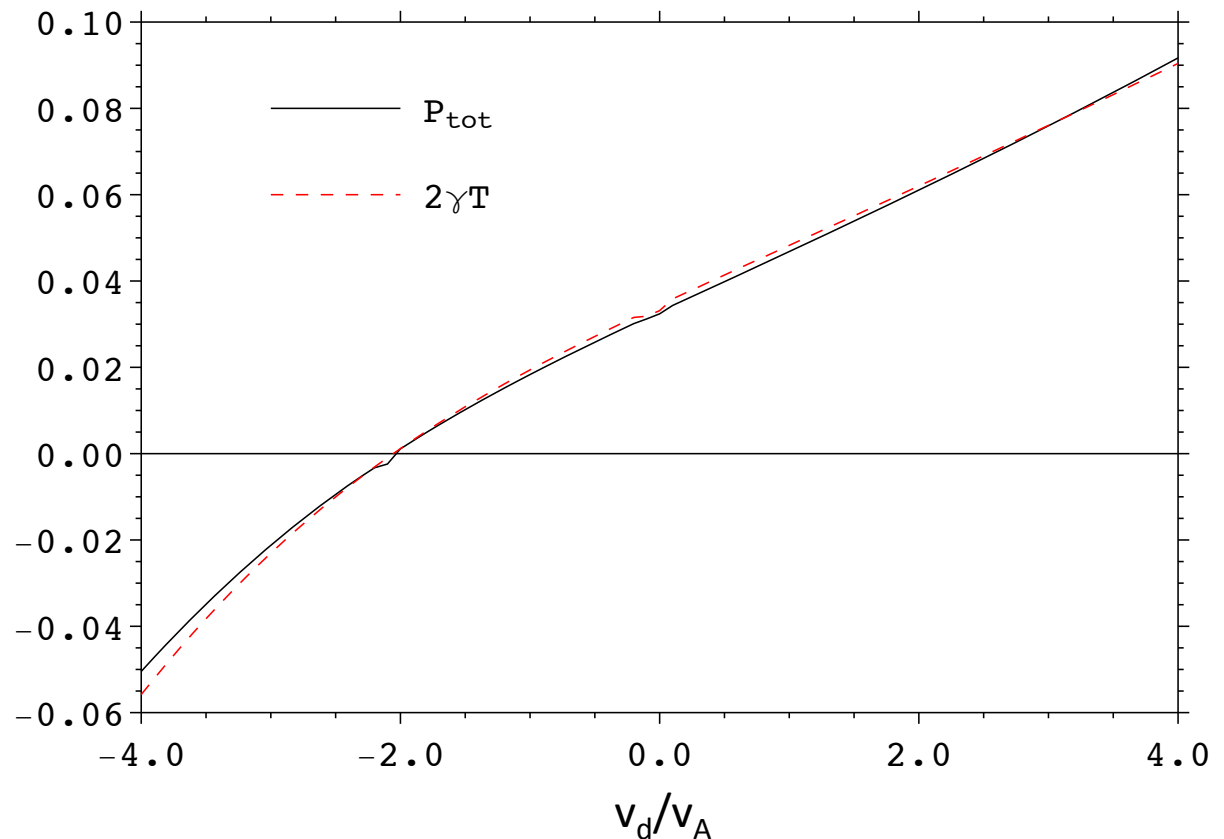


Benchmark

In the limit of weak damping/growth rates, we expect:

$$P_{tot} \equiv \sum_S P_s \approx -\frac{W(t_0 + T) - W(t_0)}{W(t_0)} \approx 1 - e^{2\gamma T} \approx -2\gamma T$$

...and we get it (here
for $k \rho_i = 0.1$)

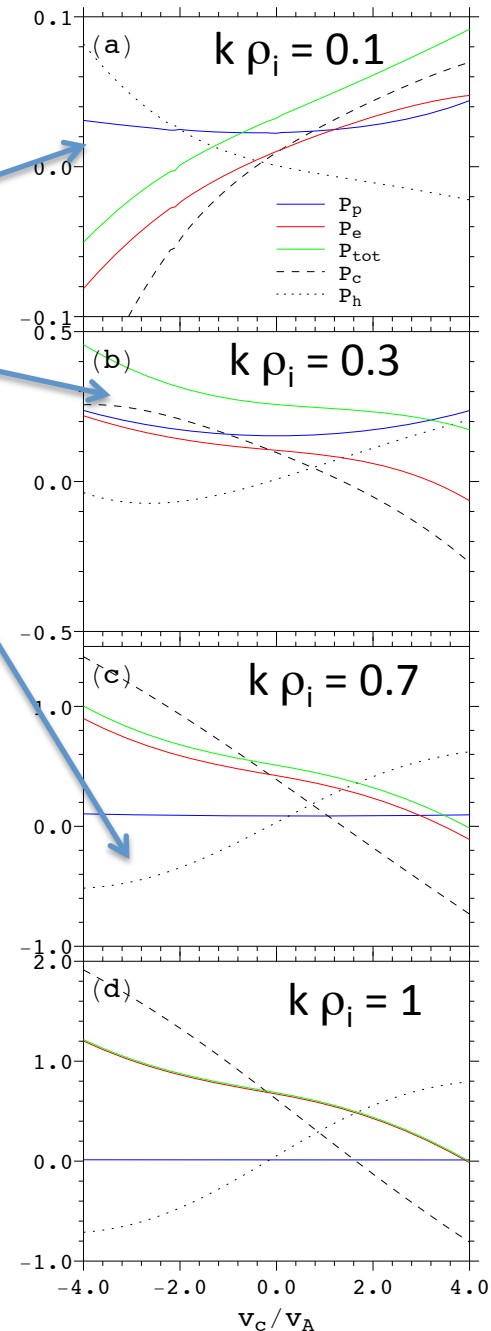
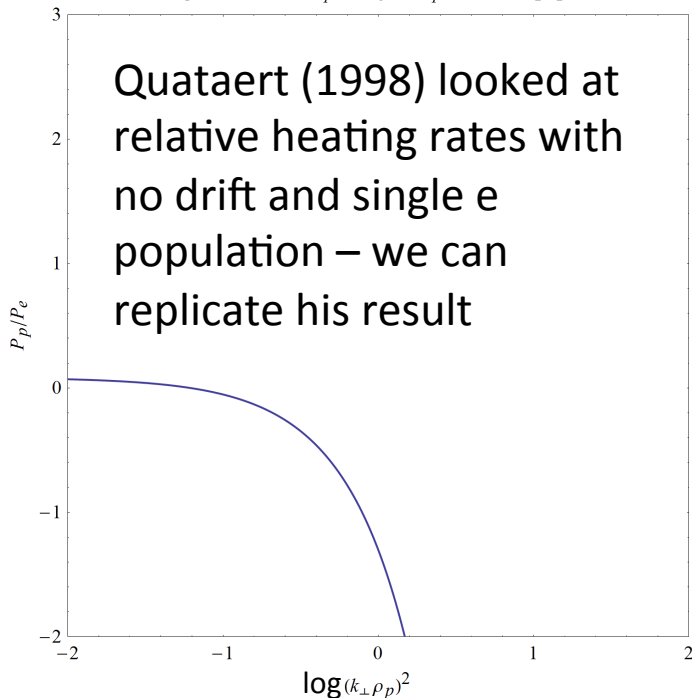


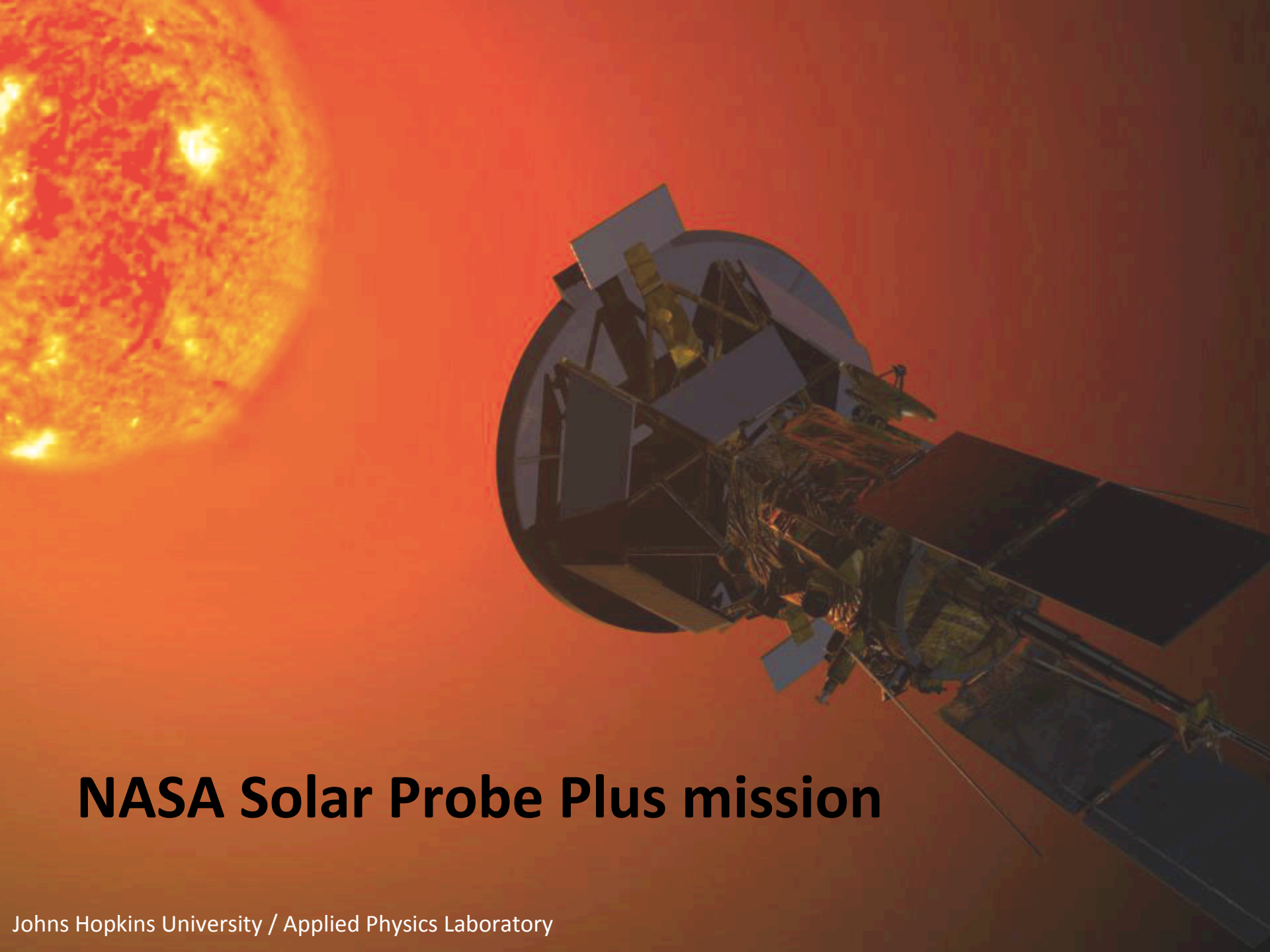
Heating rates and energy exchange

$T_c = T_i$ and $\beta_e = 1$ here

We get instability (driven clearly by core)
 We get enhanced electron heating of halo
 We get energy exchange between core and halo
 - core energy heats halo...

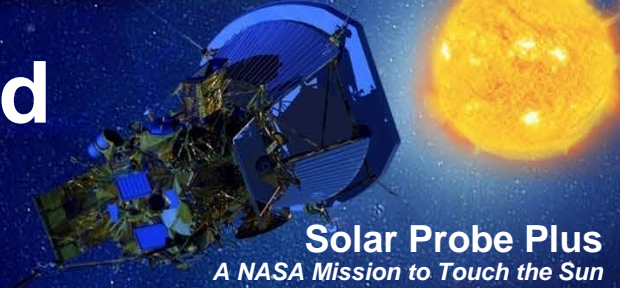
$\beta_{tot}=1.0$, the same parameter as Eliot's
 figure 1(d), $(k_\perp \rho_p)^2$ is just λ_p in Eliot's paper





NASA Solar Probe Plus mission

Reference Mission: Launch and Mission Design Overview



Launch

- Dates: Jul 31 – Aug 19, 2018 (20 days)
- Max. Launch C3: $154 \text{ km}^2/\text{s}^2$
- Requires Atlas V 551/Delta IVH class with project-provided Upper Stage

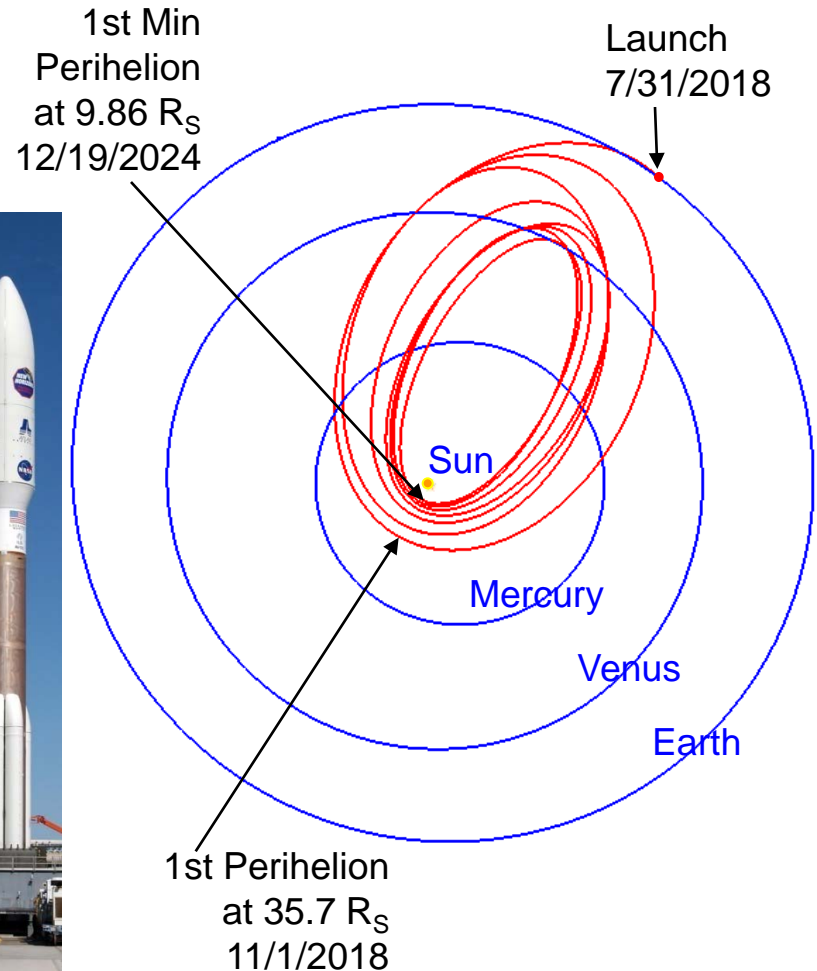
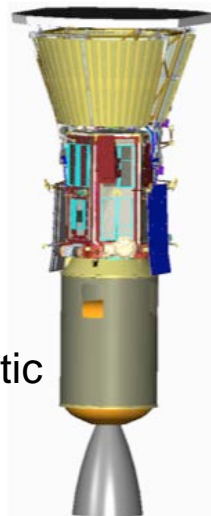
Trajectory Design

- 24 Orbits
- 7 Venus gravity assist flybys

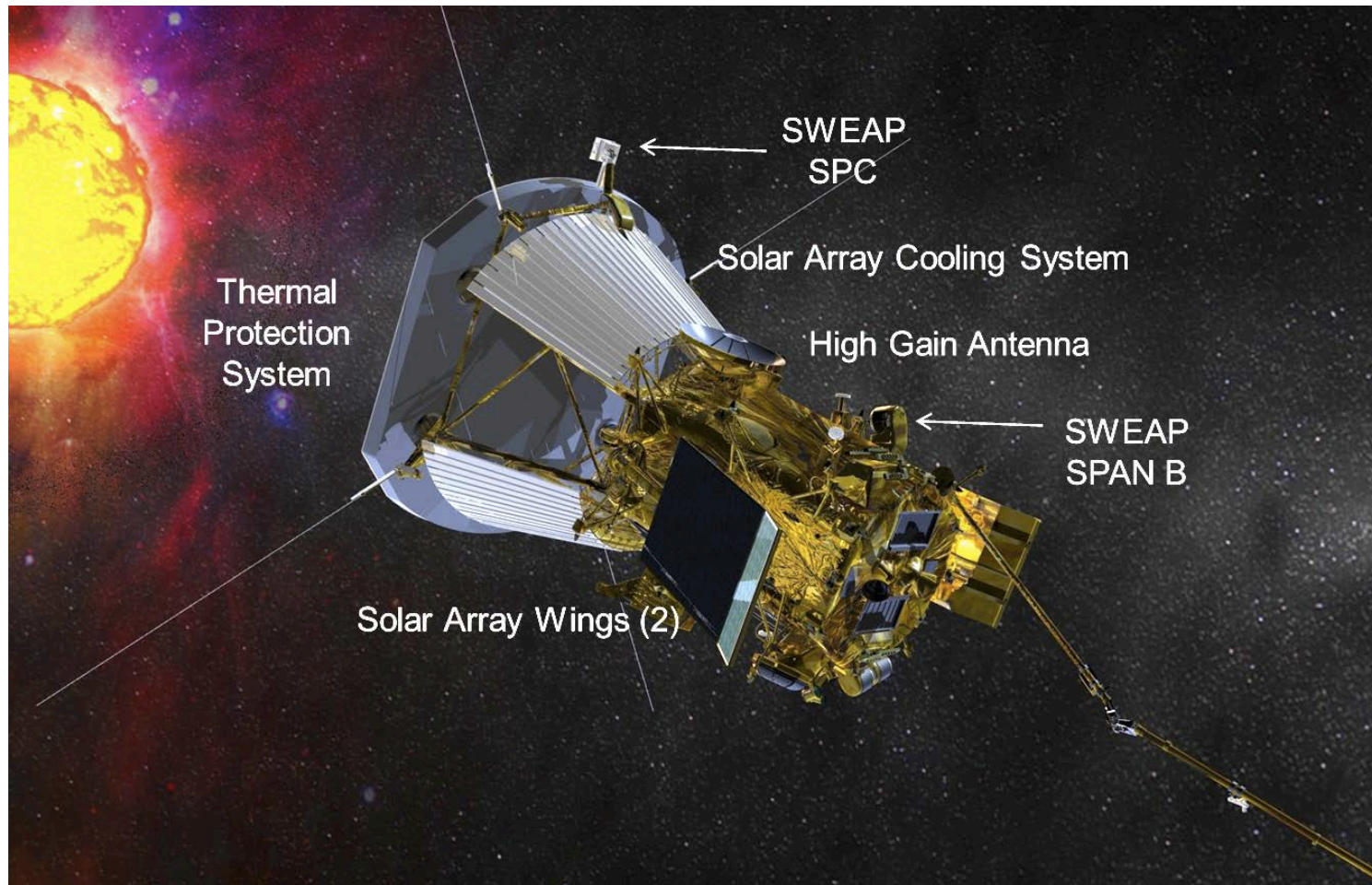
Final Solar Orbits

- Perihelion: $9.86 R_S$
- Aphelion: 0.73 AU
- Inclination: 3.4 deg from ecliptic
- Orbit period: 88 days

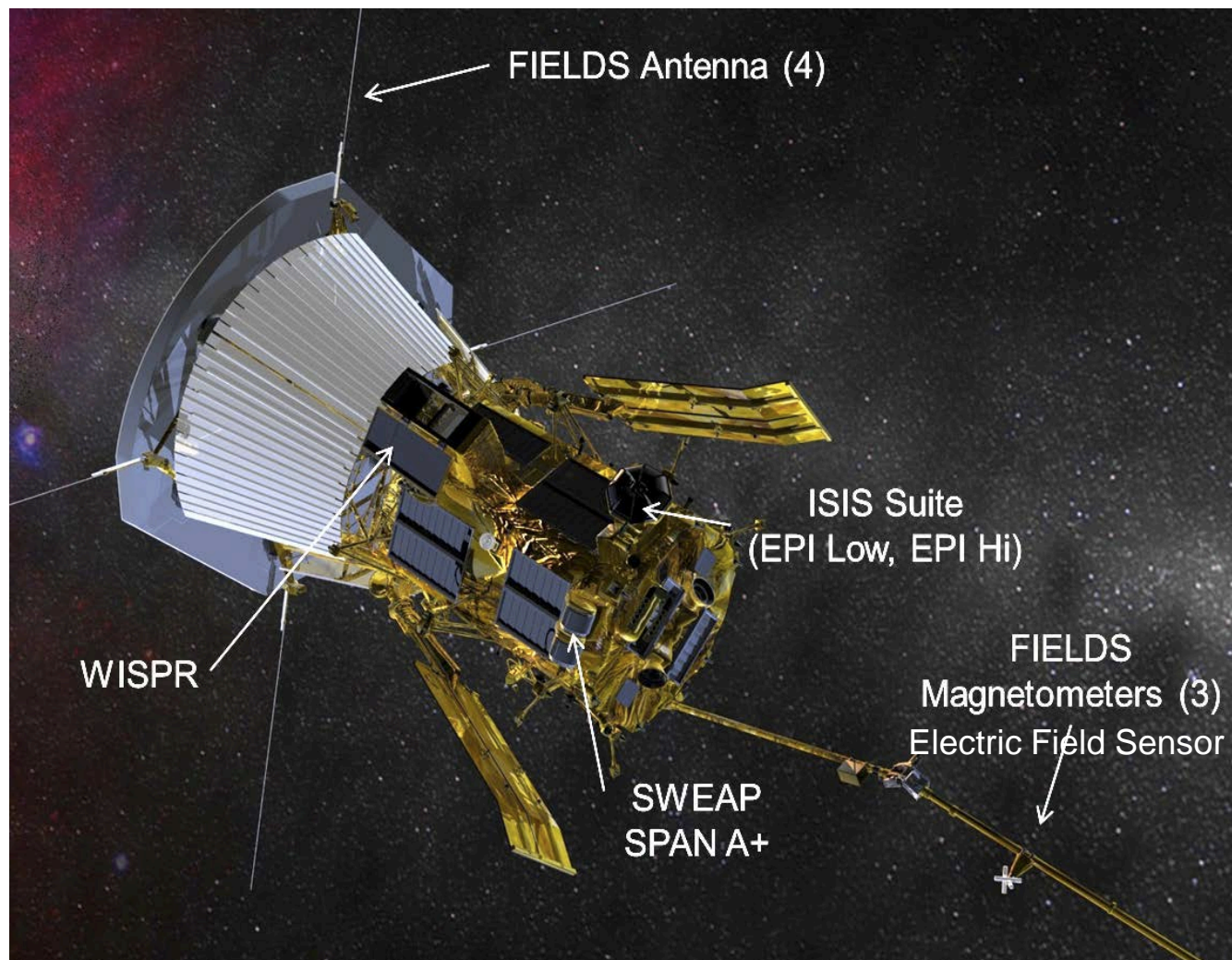
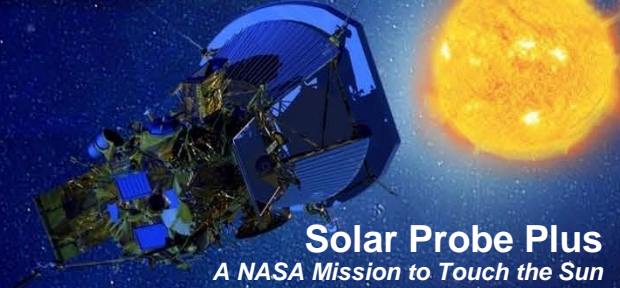
Mission duration: 7 years



Reference Vehicle: Anti-Ram Facing View



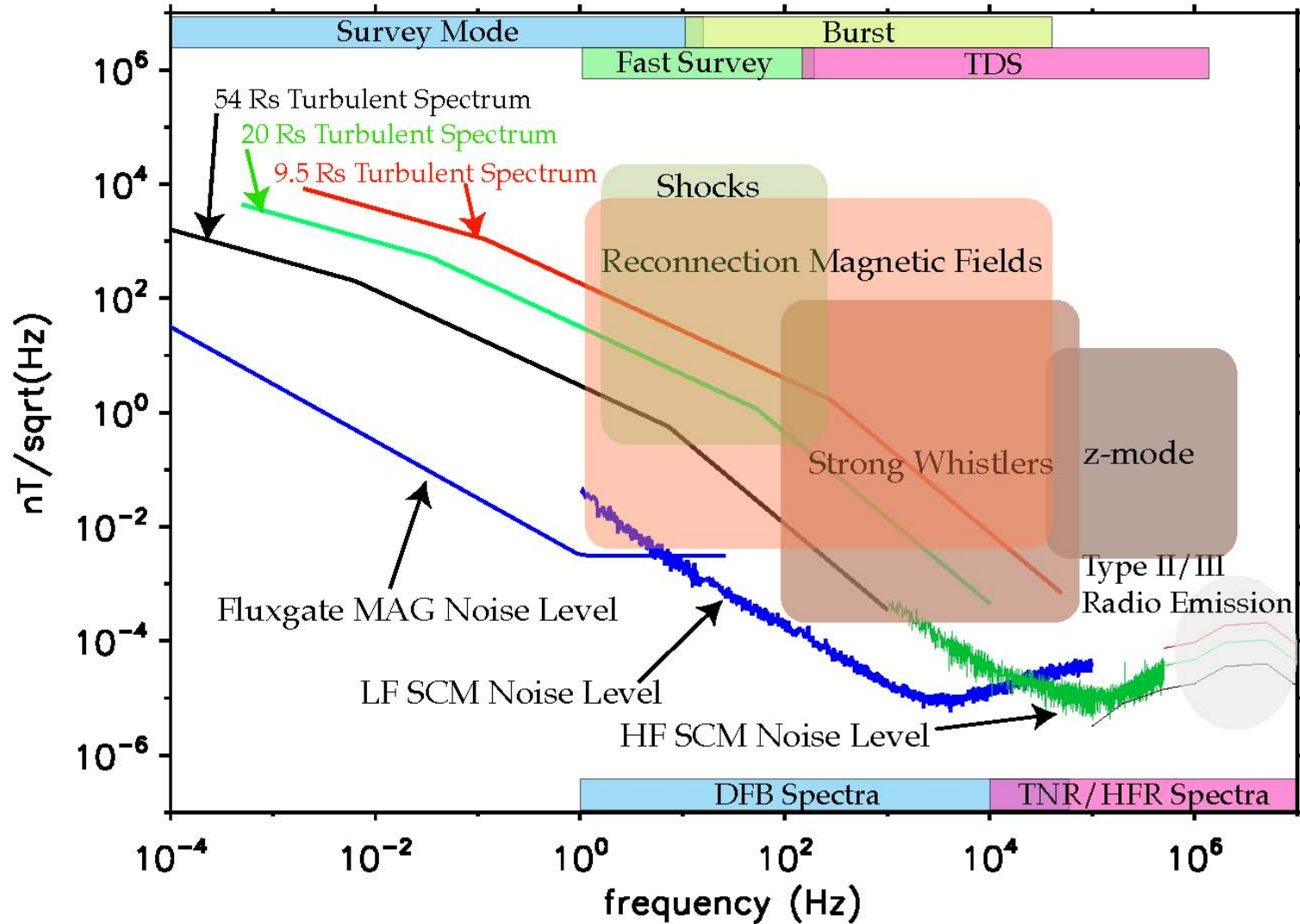
Reference Vehicle: Ram Facing View



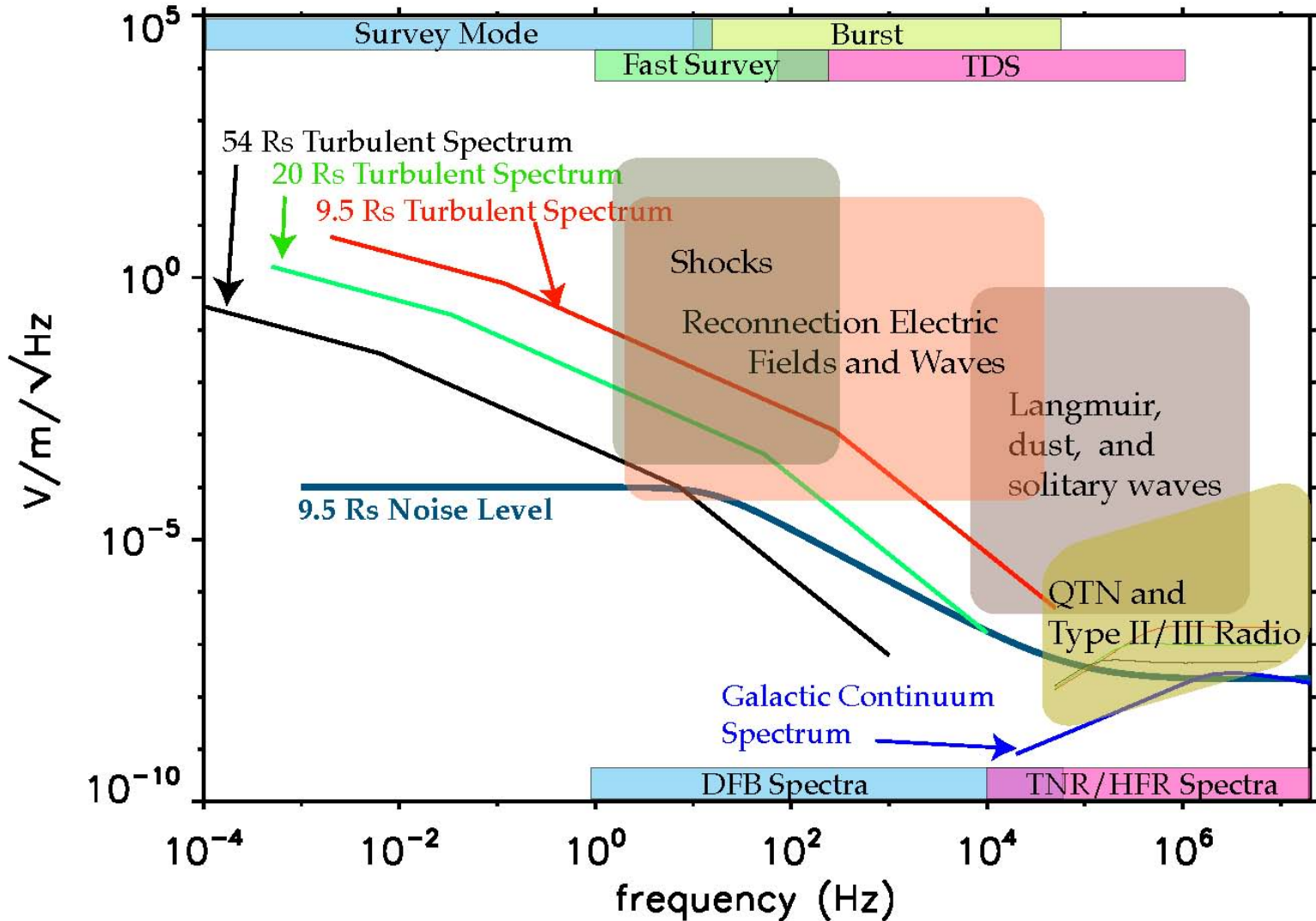
Plasma environment

Parameters		~10 R _s Typical	55 R _s Typical	1 AU Typical
Magnetic Field	$ B_0 \sim \delta B$	2000 nT	70 nT	6 nT
Electric Field	$ E \sim v_{sw} B_0$	100 mV/m	30 mV/m	3 mV/m
Density	$n_e \sim \delta n_e$	7000 cm ⁻³	120 cm ⁻³	7 cm ⁻³
Electron Temperature	T_e	85 eV	25 eV	8 eV
Solar Wind Speed	v_{sw}	210 km/s	400 km/s	450 km/s
Alfven Speed	v_A	500 km/s	125 km/s	45 km/s
Plasma Frequency	f_{pe}	750 kHz	100 kHz	24 kHz
Electron Gyrofrequency	f_{ce}	60 kHz	2 kHz	160 Hz
Proton Gyrofrequency	f_{ci}	32 Hz	1 Hz	0.1 Hz
Convected Debye Scale	v_{sw}/λ_D	250 kHz (4 μs)	125 kHz (8 μs)	45 kHz (22 μs)
Convected Electron Inertial Length	$v_{sw}/(c/\omega_{pe})$	3.5 kHz (0.3 ms)	825 Hz (1.2 ms)	180 Hz (5.5 ms)
Convected Ion Inertial Length	$v_{sw}/(c/\omega_{pi})$	75 Hz (13 ms)	20 Hz (50 ms)	4 Hz (250 ms)
Convected Ion Gyroradius	v_{sw}/ρ_i	300 Hz (3 ms)	35 Hz (30 ms)	5 Hz (200 ms)
DC/LF Electric Fluctuations	$\delta E_A \sim v_A \delta B_A$	1 V/m	10 mV/m	1 mV/m
Kinetic Electric Fluctuations	δE_L	1 V/m	70 mV/m	10 mV/m

δB fluctuation levels?



δE fluctuation levels?



end

Transition from Spitzer-Härm to a collisionless regime

Stuart D. Bale, Marc Pulupa, Chadi Salem,
Chris Chen, Eliot Quataert

University of California, Berkeley

Collisional transport theory

Spitzer-Härm (S-H) transport assumes that plasma is highly collisional:

- $f(v)$ remains \sim Maxwellian as it convects through a temperature gradient L_T
- λ_{fp}/L_T (Knudsen number) is a small parameter and required for proportionality of $q_{||}$ and dT/dr

where $q_{SH} = -\kappa_{SH} \nabla_{||} T_e$ and $\kappa_{SH} \sim 3.16 \frac{n_e T_e \tau_e}{m_e}$

...so that $\kappa_{SH} \propto T_e^{5/2}$

Then if you want constant (conductive) luminosity $L = 4\pi r^2 q_{||} = const$

you're required to have $T_e \sim r^{-2/7}$, which is in fact consistent with measurements of the radial electron temperature profile... So that's pretty compelling. This is the basis of Chapman's solar wind model (h/s equil + q)

Maximum available heat flux (in subsonic wind $v_e \gg v_{sw}$) is so-called 'saturation flux'

- $q_0 = 3/2 n k_b T v_e$ (thermal convection of full thermal energy)
- q_0 heat flux is consistent with adiabatic ($T \sim r^{-4/3}$) expansion at large radius, but not

$r^{-2/7}$

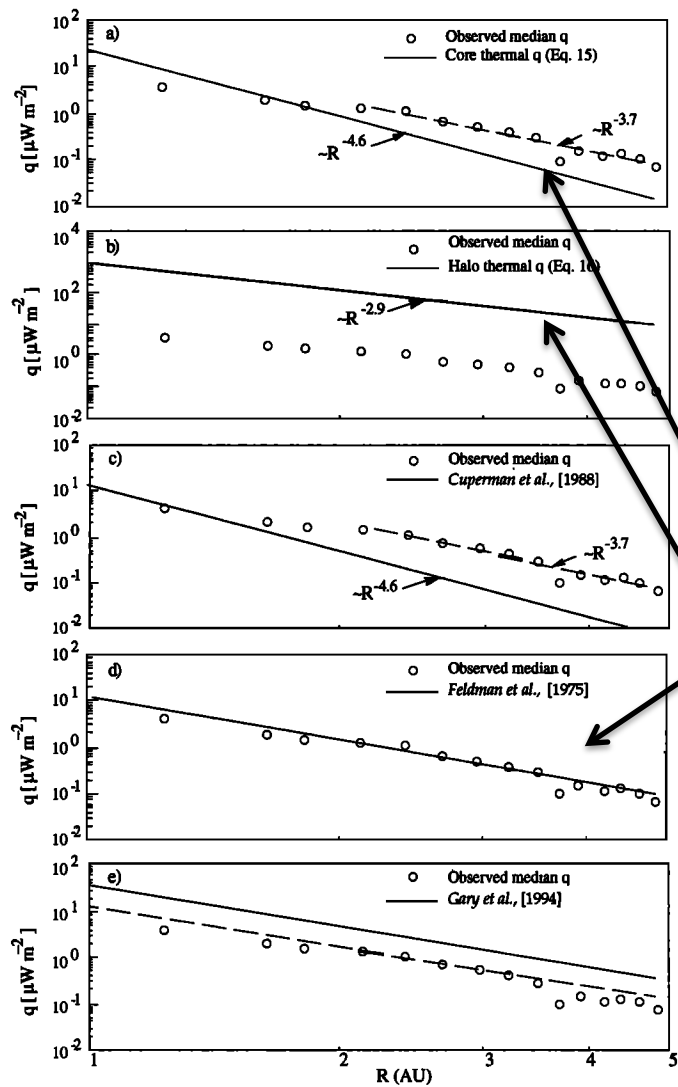


Figure 11. Ulysses observations and the (a) Thermal gradient electron heat flux based on core temperature gradient. (b) Thermal gradient heat flux based on halo temperature gradient (note different scale). (c) *Cuperman et al.* [1988] predicted electron heat flux, equation (17). (d) *Feldman et al.* [1975] bi-Maxwellian empirical electron heat flux model. (e) Solid line: whistler heat flux instability threshold, equation (23). Dashed line: modified whistler heat flux instability threshold, equation (24).

Some previous measurements

Scime et al. (1994)

'core' SH heatflux too small
'halo' SH heatflux too big
bi-Max model is just right

Feldman papers

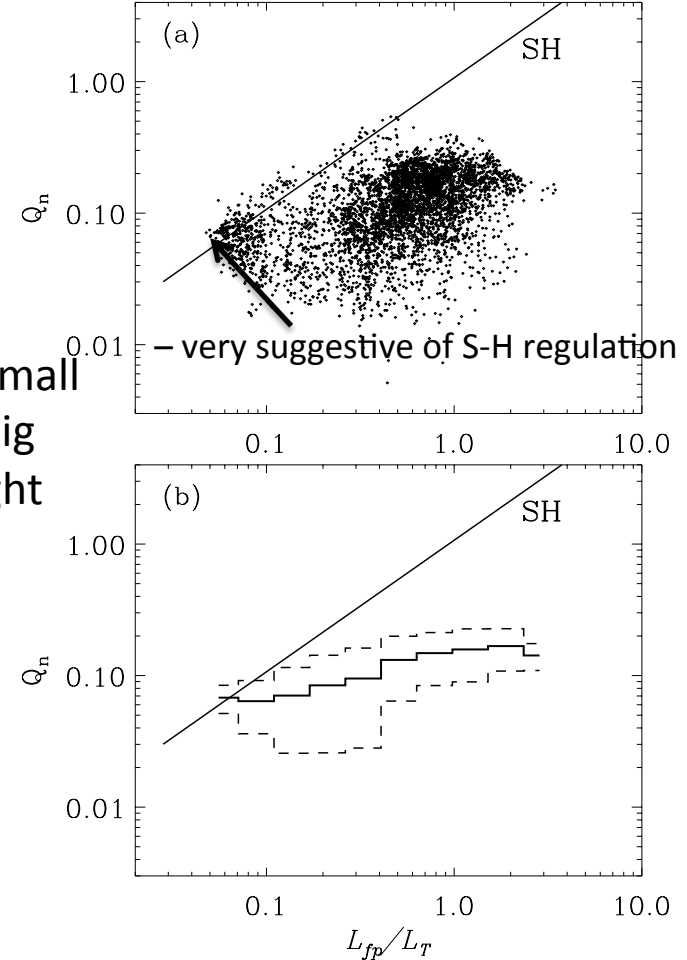


Fig. 8.—Fifty consecutive days. Eleven minute averages of the normalized heat flux Q_n (eq. [2]) in the low-pressure and free (i.e., not connected to the Earth's bow shock) solar wind as a function of the ratio between the electron mean free path L_{fp} (eq. [11]) and the scale of the temperature gradient L_T (eq. [12]). (a) Scatter plot. (b) Average m (solid line) and standard deviation σ ($m \pm \sigma$; dashed lines) in equal bins of L_{fp}/L_T . The solid line SH in both panels is the normalized heat flux predicted by the classical Spitzer-Härm collisional theory (eq. [13]).

Salem et al. (2003)

2 years of solar min
 2 years of solar max

S-H to collisionless

Modes of jPDF of $q_{||}/q_0$ vs λ_{fp}/L_T

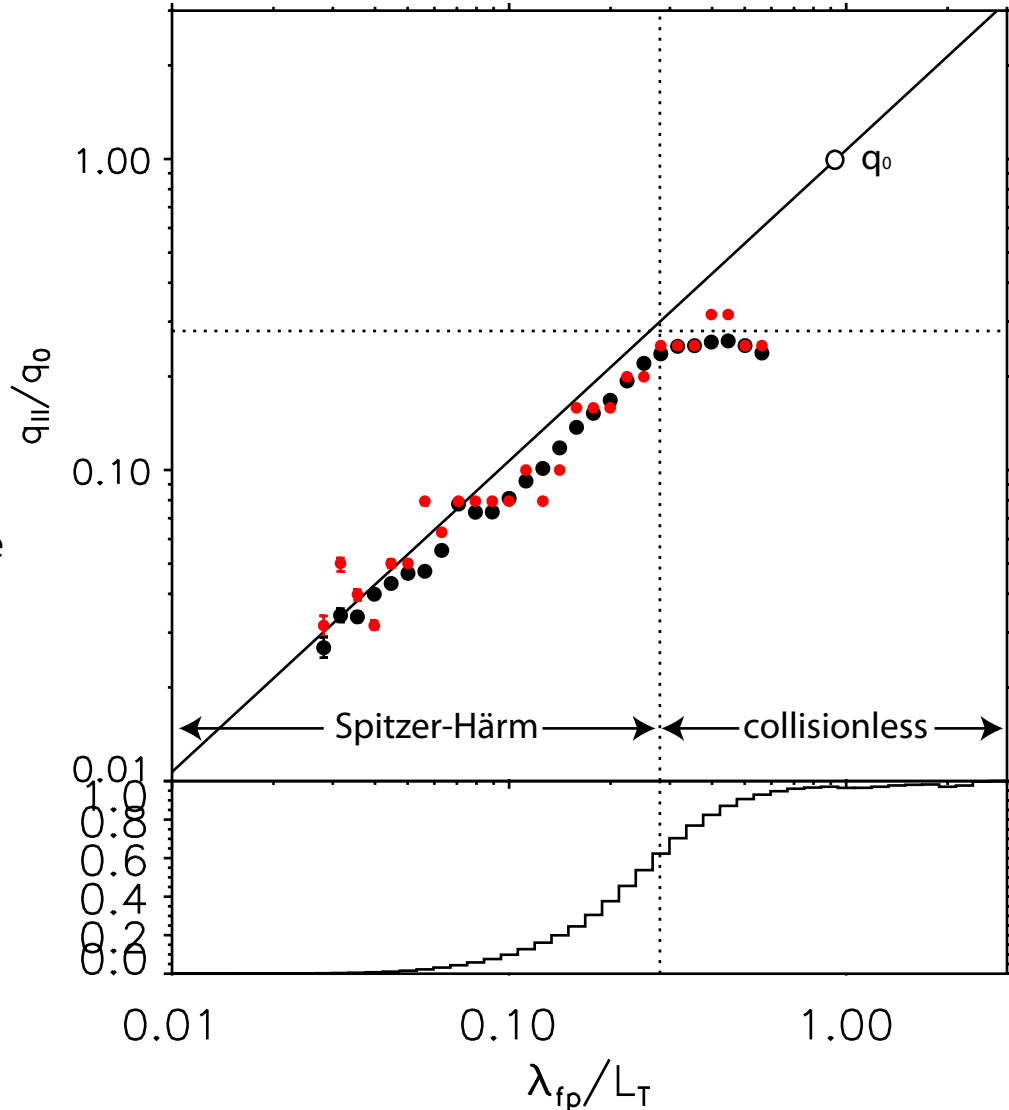
$q_{||}$ is field-aligned hf
 q_0 is saturation hf
 λ_{fp} is collisional mfp
 L_T is T_e gradient scale

65% of data is SH/collisional
 35% of data is collisionless

Collisionless limit $q_{||} \sim 0.3 q_0$
 Never reaches q_0
 This is $\alpha=2/7$ – if we fit the SH data to the curve, we get
 80% of $2/7$ ($\alpha = 0.23$ or so)
 $2/7 = \sim 0.286$
 Marsch et al., 1989

Diagonal line is:

$$\frac{q_{SH}}{q_0} = 1.07 \frac{\lambda_{fp}}{L_T}$$



β -dependence and instabilities

Gary et al (1994) marginal instability thresholds:

- whistler
- magnetosonic
- short wavelength Alfvén

These instabilities can choke off the heat flux (at the expense of wave growth)

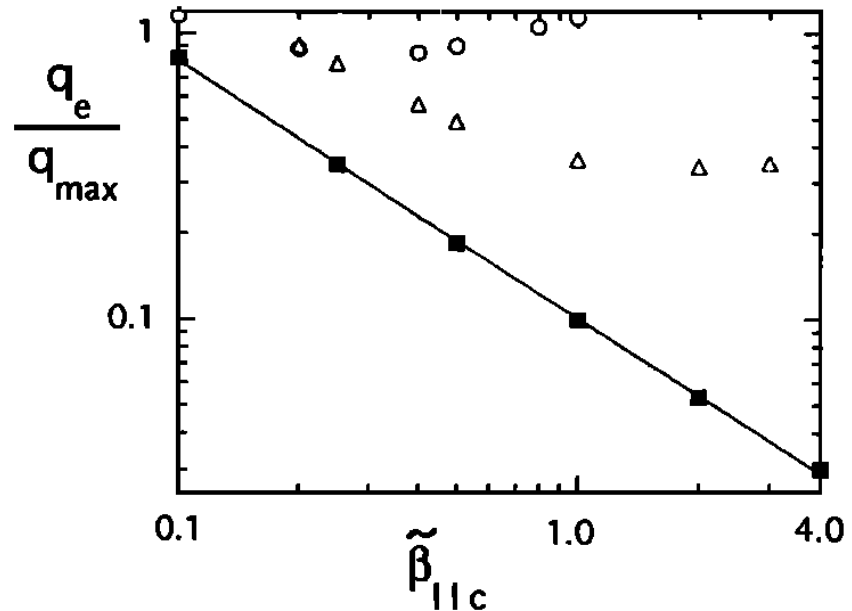


Figure 1. The dimensionless electron heat flux as a function of the parallel core β at the $\gamma_m = 10^{-3}\Omega_p$ thresholds of the whistler (solid squares), magnetosonic (open triangles), and Alfvén (open circles) heat flux instabilities. The solid line is the least squares fit to the whistler threshold, equation (3a). Unless stated otherwise, the dimensionless parameters in Figures 1 through 8 are as given in Table 1.

β -dependence and instabilities

Modes of $q_{||}/q_0$ vs λ_{fp}/L_T

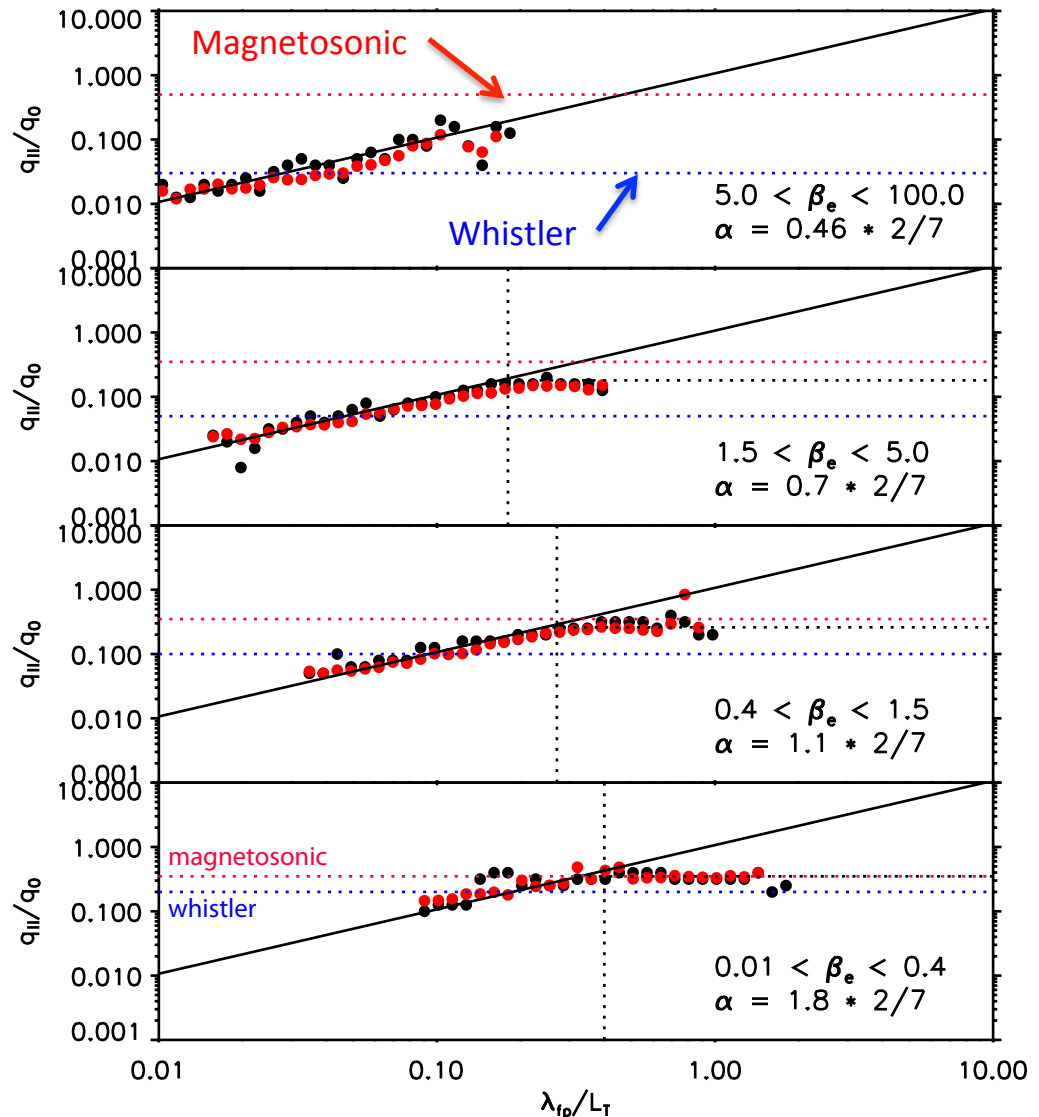
Broken into 4 intervals of electron thermal β

λ_{fp} maps to β – high β is biased to small λ_{fp}/L_T

Fit to S-H relationship requires a β -dependent α ($T \sim r^{-\alpha}$)

Gary et al (1994) marginal instability thresholds:

- whistler (blue dotted lines) *overconstrains* the data
- magnetosonic (red dotted lines) looks good in collisionless regime. Who would've thought?
- Mach number?



Flux-limited SH

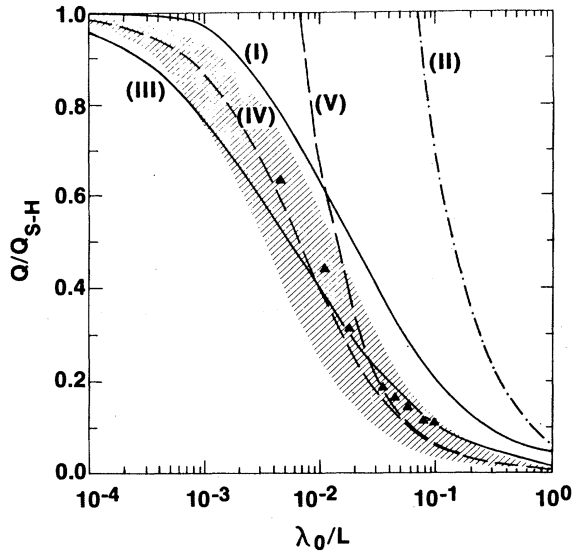


FIG. 2. Reduction of Spitzer-Härm electron thermal flux as a function of λ_0/L for $Z = 4$; Curve I, self-consistent limitation ($f_1 \leq f_0$) with a sharp cutoff (see Fig. 1); Curve II, free-streaming net flux limitation ($\alpha = 0.65$) with a sharp cutoff; Curve III, same as I with $f_1 \leq 0.75f_0$ with a harmonic cutoff; Curve IV, same as II with $\alpha = 0.06$ and a harmonic cutoff; and curve V, same as IV with a sharp cutoff. The shaded region is bounded by $0.03 \leq \alpha \leq 0.1$ using a harmonic cutoff. The solid triangles are the results from Ref. 5. Note that the λ of Ref. 5 defined at $\frac{3}{2}kT$ corresponds to $2.25\lambda_0$ here.

(Shvarts et al., PRL , 1981)

Moments of Boltzman Equation
(with $\cos(\theta)$ perturbation)

Limit f_1 to f_0 (f_1 becomes f_0 in an ad hoc way)

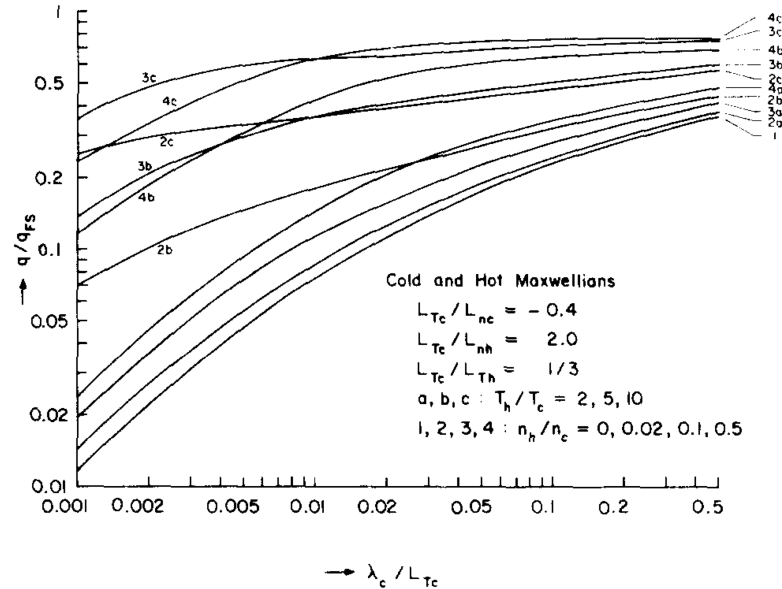


FIG. 15. Same as Fig. 9 for the second set of scale lengths.

(Shkarofsky, PoF , 1983)

Outline and Summary

- Electron velocity ‘core’ measurements
 - Old stuff – Feldman 1975, Scime 1998
 - Instability calculation – Gary 1975
- Precision electron velocity measurements
 - Wind/3DP measurements
 - Monopole spacecraft potential correction with QTN
 - $f(v_e)$ fits to core and halo
- Core electron-proton drift
 - Large drifts – in any units (v_{sw} , v_A , c_S , or even km/s!)
- Core drift modifies KAW damping rates
- Heatflux transition from Spitzer-Härm to something else

End

Core-halo resonant energy exchange

$$\zeta_s^n \equiv \frac{\omega - k_z v_s - n\Omega_s}{\sqrt{2}k_z v_{Ts}}$$

$$\zeta_s^0 \approx \frac{1}{\sqrt{2}} \left(1 - \frac{n_c v_c}{n_s v_A}\right) \sqrt{\frac{2 T_p m_e}{\beta_p T_s m_p}} \quad \text{for} \quad \omega \approx k_z v_A$$

